Heliyon 9 (2023) e22296

Contents lists available at ScienceDirect

Heliyon

journal homepage: www.cell.com/heliyon

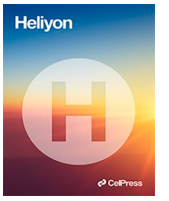

Eco-friendly concrete incorporating palm oil fuel ash: Fresh and mechanical properties with machine learning prediction, and sustainability assessment

Noor Md. Sadiqul Hasan [a], Md. Habibur Rahman Sobuz [b,*], Nur Mohammad Nazmus Shaurdho [a], Md. Montaseer Meraz [b], Shuvo Dip Datta [b], Fahim Shahriyar Aditto [b], Md. Kawsarul Islam Kabbo [b], Md Jihad Miah [c]

[a] *Department of Civil Engineering, College of Engineering and Technology, International University of Business Agriculture and Technology, Dhaka 1230, Bangladesh*
[b] *Department of Building Engineering and Construction Management, Khulna University of Engineering & Technology, Khulna 9203, Bangladesh*
[c] *Department of Civil Engineering, University of Asia Pacific, Dhaka 1205, Bangladesh*

ARTICLE INFO

Keywords:
Concrete
Cost and eCO_2 emissions
Eco-friendly
Fresh characteristics
Machine learning techniques
Mechanical performance
Palm oil fuel ash
Sustainability

ABSTRACT

Rising natural resource consumption leads to increased hazardous gas emissions, necessitating the concrete industry's focus on sustainable alternatives like palm oil fuel ash (POFA) to replace cement. Also, advanced machine learning (ML) techniques can uncover previously unreported insights about the effects of POFA that may be missing from the literature. Hence, this study investigates the influence of varying concentrations of POFA on fresh and mechanical characteristics with quantifying ML approaches and microstructural performance, as well as the environmental impact of structural concrete. For this, cement substitutions of 5 %, 15 %, 25 %, 35 %, and 45 % (by weight of cement) were utilized. POFA enhanced the overall concrete workability, with slump increments ranging from approximately 9 %–55 % and compacting factor increments of 4 %–12 %. Mechanical performance of POFA concrete improved up to 25 % replacement levels, with the highest enhancements observed in compressive (4.5 %), splitting tensile (36 %), and flexural (31 %) strength, for the mix containing 15 % POFA. The finer particle size of POFA improved microstructural performance by reducing porosity, aligning with the enhanced mechanical strength. The environmental impact of POFA was assessed by measuring eCO_2 emissions, revealing a potential reduction of up to 44 %. Incorporating 5 %–15 % POFA yielded ideal mechanical performance results, significantly enhancing sustainability and cost-effectiveness. Regarding the ML approach, it can be observed that a low regression coefficient (R^2) contrasts sharply with the higher R^2 values for the random forest (RF) and the ensemble model, indicating satisfactory precision prediction with experimental results.

1. Introduction

The concrete industry faces a worldwide challenge, as it consumes many resources while emitting CO_2 gas at a high volume [1,2].

* Corresponding author. habib@becm.kuet.ac.bd (M.H.R.S).
E-mail address: habib@becm.kuet.ac.bd (Md.H.R. Sobuz).

https://doi.org/10.1016/j.heliyon.2023.e22296
Received 11 August 2023; Received in revised form 8 November 2023; Accepted 9 November 2023
Available online 15 November 2023

The manufacturing and consumption of cement have increased with the ongoing rise in the need for and usage of concrete in various construction activities [3,4]. According to Aprianti [5], it is possible to produce almost 1 ton of CO_2 from one ton of cement. There is a need to give attention towards sustainability in the construction sector [6]; hence, the investigation into diverse supplementary cementitious materials (SCM) has remained a persistent subject of scholarly inquiry [7–11]. The assessment of the impacts of various SCMs, and their interactions with additional reinforcing agents such steel fiber [12], glass fiber [13], lightweight [14] and heavyweight aggregates [15], has also been carried out. In recent years, numerous studies by different researchers have emerged indicating the application of agro deposits throughout the concrete industry [16–20]. Palm oil fuel ash (POFA), a byproduct of palm oil production, is generated through burning waste products like palm oil shells, fibre, kernels, as well as empty bunches of fruits inside reactors [21]. The utilization of POFA as a replacement for cement content in concrete mixtures is justified by its accelerated pozzolanic reactivity attained by heat treatment [22,23]. Palm oil factories produce the fuel ash substantially with time due to the rising demand for POFA [24]. The Malaysian industry generates approximately 3 million tons of POFA annually, while Thailand's average production rate is more than 100,000 tons yearly [25]. For every 8 kg of raw palm oil batch, a maximum of 2 kg of palm oil can be produced, and the rest is characterized as dry biomass [26]. Disposal of this waste residue into open land and use as landfilling constituents without any further treatment can affect humans causing several diseases [26]. The geopolymer characteristics of POFA make it more environmentally friendly and consume less energy to manufacture compared to traditional materials [27]. As a result, sustainability and cost-effectiveness can be achieved by replacing a certain volume of cement quantity with POFA, which also could reduce the transportation cost and waste materials in landfills [28,29].

The fineness of POFA is considered the most significant factor affecting the strength alongside the durability characteristics of concrete [30]. Multiple researchers are examining how increasing POFA fineness and its pozzolanic reactivity enhances concrete strength [31,32]. In the 1990s, Tay [33] studied the POFA properties as a concrete material by incorporating POFA in place of ordinary Portland cement (OPC), which ranges from 10 % to 50 % of cement replacement. Later, numerous studies showed different results enhancing the concrete properties [34–36]. The study of Kroehong et al. [37] in 2011 emphasized the fineness impacts of POFA upon this pozzolanic response of cement paste. They replaced cement weight by 10 %, 20 %, 30 %, and 40 % of Ground Palm Oil Fuel Ash (GPOFA) and Ground River Sand (GRS). The authors concluded that a higher reaction rate and higher concrete strength with the increment of POFA fineness is presented in the mix and also observed the presence of high silica content. The reaction rate enhancement because of the presence of silica content was also observed by various researchers [38,39]. The study of Chindaprasirt et al. [40] concluded the enhancement of workability and mechanical performances with the 20 % OPC replacement by POFA. The study also reported the strength's decrement pattern due to the increased water usage requirement at 40 % cement replacement by POFA. Around 11 % increment of compressive strength was evaluated in the examination of Sata et al. [41]. The examination of Tangchirapat et al. [42] also suggested an increment of 8 % with a similar kind of replacement. The optimum strength increment pattern was evaluated in 10–20 % of POFA replacements [43,44]. High-volume POFA concrete reduced CO_2 emissions by 32–45 % and the cost of manufacturing by 8–12 % compared to cement-based concrete. It leads to energy savings and reduced consumption of natural resources, shifting the focus of the concrete industry toward a greener, more environmentally sustainable method of manufacturing [43,45].

As the field of artificial intelligence (AI) has progressed, machine learning (ML) approaches have been used to make predictions about various mechanical and physical properties of concrete [46]. Several ML methods, including clustering, regression, and classification, may be utilized to provide reliable predictions of compressive strength by quantifying a wide range of other characteristics [47–49]. With the use of gene expression programming (GEP), Javed et al. [50] predicted the compressive strength of concrete made from sugarcane bagasse ash (SCBA). Naderpour et al. [28] used an artificial neural network (ANN) to foretell the recycled concrete's mechanical characteristics. Similarly, Getahun et al. [51] implement ANN to predict the longevity of concrete that includes wasted components. Improving model performance is a perennial goal and source of tension in the dynamic field of machine learning. In an effort to improve forecast accuracy and generalisation, several methods have been developed and refined. Among them, Random Forest and Artificial Neural Networks (ANNs) have emerged as two of the most popular and successful approaches. By combining the two, or strategically deploying models depending on the features of the task at hand, researchers have been able to achieve previously unimaginable levels of success with machine learning. Applying these techniques alone or integrating them in innovative ways has shown to be a revolutionary approach for optimizing performance gains in ML models, hence dramatically expanding the models' applicability to a wide range of use cases and data sets.

1.1. Research Significance and objectives

This study delves into the behavior of concrete when a substantial portion of traditional cement is substituted with palm oil fuel ash (POFA). It uniquely combines the integration of sustainability assessment and advanced data acquisition techniques, all while employing significant concentrations of POFA. What truly distinguishes this research is its groundbreaking approach, the application of state-of-the-art machine learning methods, including the formidable random forest (RF) and artificial neural network (ANN), for the prediction of fresh and mechanical properties in POFA-treated concrete. Such an approach is unprecedented in the field and promises to revolutionize our understanding of this innovative material. Also, the present research meticulously incorporates carbon emission data and performs an exhaustive battery of tests, thereby establishing new standards for empirical rigor. The percentages of POFA utilization are systematically varied in these tests, enabling robust correlations and comparisons to be drawn against established industry benchmarks. The dual-pronged mission is as follows: first, addressing pressing environmental concerns by advocating for a reduction in cement consumption. This not only minimizes the need for extensive POFA landfill disposal but also serves as an effective strategy to mitigate the carbon dioxide emissions associated with traditional cement production. Simultaneously, our second objective

is to provide a comprehensive predictive framework for assessing the performance of POFA-treated concrete. ML algorithms have revolutionised the prediction of concrete strength by providing more precise forecasts than conventional approaches could ever achieve by identifying detailed patterns and correlations from massive datasets. These models also aid sustainable building practises by minimising material waste while maximising concrete mix design strength. Overall, machine learning improves the precision and speed with which predictions of concrete strength may be made, leading to better building practises. In essence, this research represents a transformative leap toward fostering sustainability and predictive precision in the realm of innovative structural concrete technology.

2. Experimental program

2.1. Materials

Ordinary Portland cement (OPC) CEM Type-I 52.5 N produced from the local market complying with ASTM-C150 [52], and the fuel ash of palm oil gathered from the boiler of a local palm oil factory were employed as binders. The burning temperature is considered the main factor affecting the physical properties of POFA [53,54]. POFA is generally grey, but the grey becomes darker because a substantial volume of unburned carbon is present [55]. When it is burnt furthermore, the maximum amount of carbon particles can be removed; as a result, the colour changes from darker ash to light grey. Fig. 1(a and b) depict the raw POFA and SEM image of the POFA that was utilized in this investigation. The morphology of POFA was identified through Fig. 1b, indicating that POFA consists of spherical and irregular particles in shape with a sizable fraction and porous, cellular structure. In the concrete mixes, river sand was used as the fine aggregate, while stone chips with a 12 mm maximum size were employed as coarse aggregates. The raw samples of OPC, fine aggregate and coarse aggregate used for specimen preparation are depicted in Fig. 2(a–c). The gradation curve of fine and coarse aggregates is shown in Fig. 3a, which complies with the ASTM-C33 [56] standard. The gradation curve of fine and coarse aggregates is a graphical representation of the particle size distribution of the aggregate materials used in construction. The fineness modulus of fine aggregate is 2.67, whereas coarse aggregate has a fineness modulus of 5.94. The gradation curve for fine and coarse aggregates met specific requirements for the intended use. The particle distribution of size curves for OPC and POFA is displayed in Fig. 3b. The overall grain size of POFA was lowered from 61.7 to 10.2 mm after grinding, and a change from 40.2 % to 1.6 % was made to the quantity retained on sieve No. 325.

The X-ray diffraction pattern of POFA at 1100° Celsius is depicted in Fig. 4. Sharp spikes at 22° and 25.5° suggest the presence of crystalline cristobalite and silica in tridymite form [57]. Various factors affect the chemical composition of POFA, including the heat at which it burns, how effectively it burns, and the components of the palm oil used in different factories [58].

Table 1 shows the chemical composition of OPC CEM Type-I and POFA that was obtained by XRF analysis. The presence of SiO_2, which is the main composition of POFA, ranges between 44 % and 72 %, which gives good pozzolanic properties to the POFA particles [59].

As can be seen in Table 2, different aggregate parameters were ascertained using ASTM-C29 M [60], ASTM-C127 [61], ASTM-C128 [62], and ASTM-C136 [63] standards. In addition, ASTM-C494 [64]-compliant Type-A water-reducing superplasticizer was used in this study.

2.2. Mix proportioning of the sample

The concrete batches were mixed using a 90 L electric-powered concrete mixing machine. The coarse aggregates were first placed into the mixer machine to produce the concrete specimens, then sand and cement, respectively. For 1.5 min, the components were equally blended under dry conditions. After adding water, the mix continued for 3.5 min until flowability was achieved visually. Finally, a superplasticizer was added until the mixture became homogeneous. ASTM-C192 [65] standard was followed throughout the entire mixing process. The mix proportion of the ingredients is displayed in Table 3.

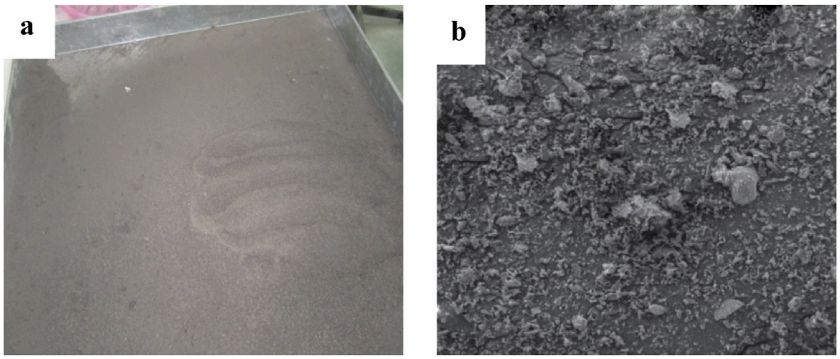

Fig. 1. (a) Raw POFA ash (b) SEM image of POFA particles.

Fig. 2. Samples of raw materials used: (a) OPC, (b) fine aggregate, and (c) coarse aggregate.

2.3. Procedure for preparing samples and curing

Fig. 5(a–d) show the method of preparaing concrete specimens and their curing method. The 100 mm × 200 mm concrete cylinders were cast to prepare the samples for compressive strength, as depicted in Fig. 5a and the demoulded cylinders were shown in Fig. 5b. Prisms with measurements of 100 mm × 100 mm × 500 mm were casted and prepared for testing the flexural strength, as shown in Fig. 5c. During this sample preparation process, the molds were lubricated properly with lubricants. Then after filling up the molds, they were appropriately identified for future identification. After 24 h, the samples were de-molded carefully so that the surface was not harmed. After removing the concrete molds, the samples were cured in water tank until the preferred test day, as represented in Fig. 5d. To conduct the hardened properties tests, the specimens were cured in water curing tanks for 7 days, 14 days, and 28 days at 25 ±2 °C. The preparation and curing procedure was done complying with the ASTM-C192 [65] standard specified guidelines.

2.4. Testing of fresh and mechanical properties

The ASTM-C143 [66] standard was followed to conduct the slump cone test to evaluate fresh concrete's workability. Additionally, the mixture's yield stress as well as plastic viscosity characteristics significantly impact the concrete slump. Hu et al. [67] created a formulation for measuring slump yield stress and concrete density using finite element analysis to perform a slump flow test. This expression is shown in equation (1). The concretes having slumps in the range of 0–250 mm were subjected to finite element analyses. The formula is inappropriate for concretes exhibiting a plastic viscosity higher than 300 Pa s [68]. Compacting factor test was conducted maintaining BS-EN-12350-4 [69] guidelines, while BS-EN-12350-6 [70] was followed to determine the density of fresh concrete.

$$\tau_0 = \frac{\rho}{270}(300 - S) \tag{1}$$

where, τ_0 = Yield stress (Pa); ρ = Fresh density (kg/m^3); and S = Slump value (mm).

Compressive, flexural, and splitting tensile strength were assessed after curing for 7, 14, and 28 days. The test for compressive strength was executed following ASTM-C39 [71], while the splitting tensile strength test and flexural strength assessments were executed in compliance with ASTM-C496 [72] and ASTM-C78 [73], respectively. To determine the mechanical properties, 108 concrete cylinders were made for the compression and tension test, and 54 concrete prism specimens were cast for the flexure test.

2.5. Machine learning techniques

Following the unveiling of the concept of the machine learning (ML)approach, an in-depth contrasting model was developed to predict the fresh and mechanical properties of the POFA-treated concrete. The random forest (RF) and the artificial neural network (ANN), were utilized in the present investigation. Equations (2)–(4) quantify the model's accuracy on several criteria. The flowchart utilized for the predictive model investigation is presented in Fig. 6.

$$\text{Mean Square Error, MSE} = \frac{1}{n}\sum_{i=1}^{n}(Y - Y_i)^2 \tag{2}$$

$$\text{Root Mean Square Error, RMSE} = \sqrt{\frac{1}{n}\sum_{i=1}^{n}(Y - Y_i)^2} \tag{3}$$

$$\text{Mean Absolute Error, MAE} = \frac{1}{n}\sum_{i=1}^{n}|Y - Y_i|^2 \tag{4}$$

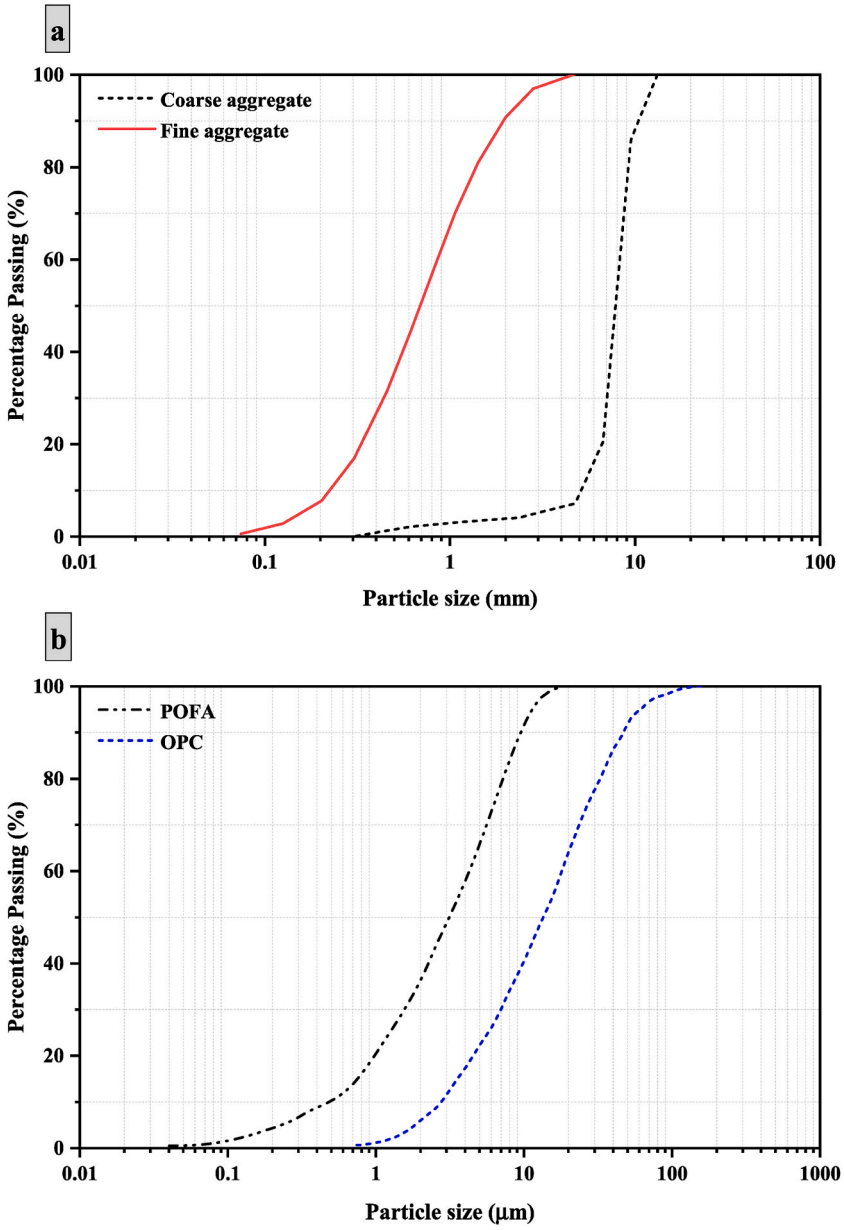

Fig. 3. Particle distribution curve (a) fine and coarse aggregates (b) OPC and POFA.

Leo Breiman and Adele Cutler developed Random Forest, a highly effective machine-learning method, in 2001. It accomplishes its goal by building several decision trees, each trained on a unique subset of the data and considering a different random selection of characteristics at each splitting point. RFs provide reliable and accurate outcomes by averaging or voting on the forecasts of many individual trees. By taking into account a wide variety of characteristics and their relative relevance, it reduces the risk of overfitting and improves prediction accuracy. This ensemble method excels in situations involving complicated, high-dimensional datasets because of its ability to robustly handle noisy data and missing values.

The Artificial Neural Network (ANN) is a kind of computational model replicating how real neural systems operate in the brain. Warren McCulloch and Walter Pitts initially introduced the proposal of artificial neurons with connections to each other in the 1940s. ANNs are an effective method for addressing various challenges in the technological and scientific communities. It is extensively utilized in the context of creating statistical frameworks for predicting the outcomes of complex, nonlinear processes. ANNs make use of deep learning architectures to automatically extract hierarchical features from the input, which may greatly improve model performance. During training, ANNs repeatedly adjust their parameters using methods like backpropagation and gradient descent, increasing their precision with each iteration.

The decision between Random Forest and ANN in practice often hinges on the nature of the issue, the size of the dataset, and the

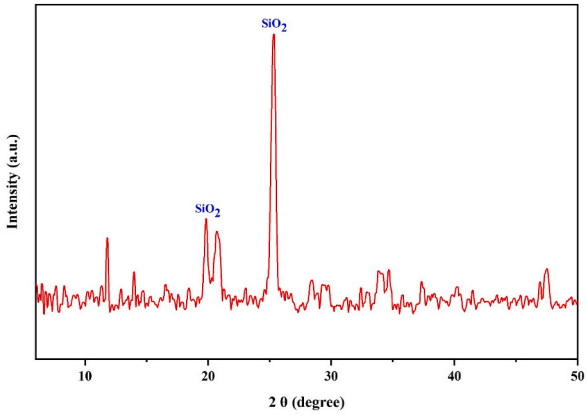

Fig. 4. XRD pattern of POFA.

Table 1
Composition and comparison between the chemical properties of POFA and OPC.

Chemical composition	OPC (%)	POFA (%)
Al_2O_3	4.02	3.73
SiO_2	17.6	64.17
CaO	67.43	5.8
Fe_2O_3	4.47	6.33
K_2O	0.39	8.25
Na_2O	0.03	0.18
MgO	1.33	4.87
SO_3	4.18	0.72
LOI	–	5.95

Table 2
Physical properties of aggregates.

Aggregate	Density (kg/m^3)	Fineness modulus	Moisture content (%)	Void (%)	Water absorption (%)	Specific gravity		
						Dry	SSD	Apparent
Fine	1565	2.67	2.36	30.97	1.36	2.41	2.44	2.48
Coarse	1682	5.94	1.87	38.12	1.14	2.76	2.79	2.83

Note: SSD: Saturated surface dry.

Table 3
Mix proportions of all concrete mixes.

Mix ID	Cement (kg/m^3)	Fine aggregate (kg/m^3)	Coarse aggregate (kg/m^3)	POFA (kg/m^3)	water to cement ratio	Superplasticizer (l/m^3)
0 % POFA	450	682	1023	0	0.23	16.5
5 % POFA	427.47	682	1023	22.53	0.23	16.5
15 % POFA	382.41	682	1023	67.59	0.23	16.5
25 % POFA	337.36	682	1023	112.64	0.23	16.5
35 % POFA	292.3	682	1023	157.7	0.23	16.5
45 % POFA	247.24	682	1023	202.76	0.23	16.5

accessibility of computing resources. While ANNs excel at jobs involving huge amounts of unstructured data and sophisticated patterns, RF is often a strong option for smaller datasets with unambiguous feature values.

3. Results and discussion

3.1. Fresh properties

3.1.1. Slump and density

Fig. 7 depicts the pattern of slump and density for the concrete mixtures. It was noticed that the addition of POFA steadily increased

Fig. 5. Preparation of concrete specimens: (a) casting, (b) cylindrical, and (c) prism specimens, and (d) curing method.

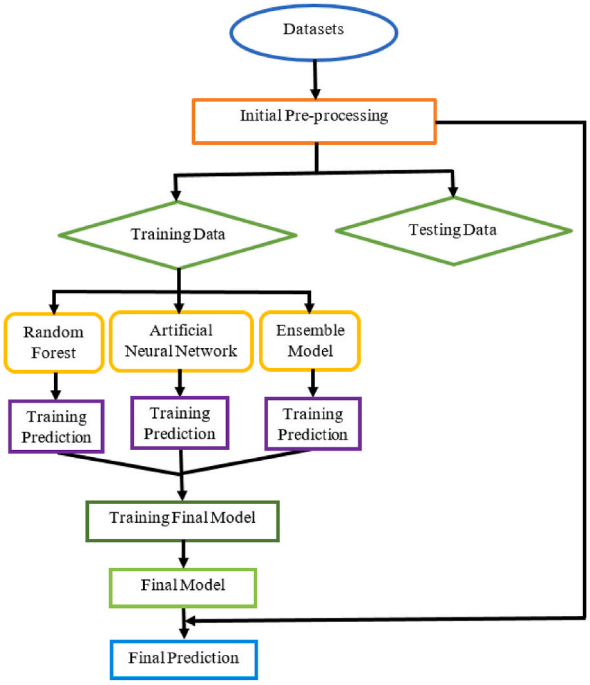

Fig. 6. Illustration of the suggested ML approach methodology.

the workability of concrete, where the graph depicts a decreasing density pattern. According to Figs. 7 and 45 % POFA replacement depicted a maximum slump value of 99.3 mm, representing a 54.36 % improvement compared to the control mixture (containing 0 % POFA). The control mix showed the lowest slump value of 64.33 mm. In addition, the slump value increased by more than 25 % with a 35 % replacement of POFA. This could be due to the greater binder volume as the specific gravity of POFA is lower than cement, and the excess binder volume could have provided better coating, lubrication, and filling of gaps in the aggregates, thus providing ease of movement and rolling of concrete particles effortlessly, resulting in a higher slump. In addition, the enhancement in workability of concrete mixes cast with POFA could be associated with lesser carbon inertia and lesser ignition losses remaining in POFA, particularly when the substitute percentage of OPC is relatively high [74]. Aldahdooh et al. [75] and Awal and Shehu [76] observed the same pattern due to the replacement by POFA. Also, the study of Alsubari et al. [45] and Salam et al. [77] exhibited a similar pattern for

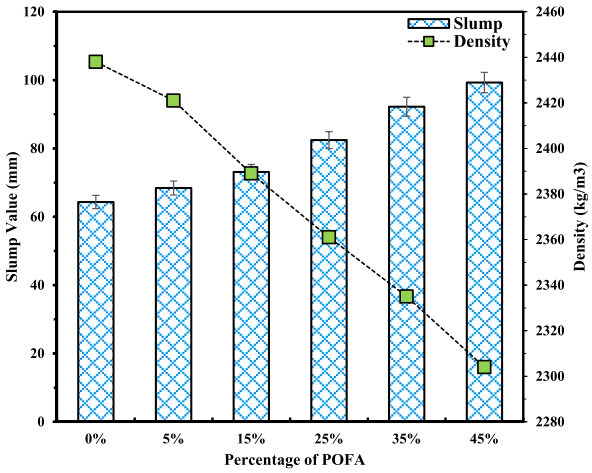

Fig. 7. Average slump and density of concrete mixes.

producing POFA-based high-strength and self-consolidating concrete. Furthermore, as a significant amount of OPC was replaced with POFA (i.e., 45 %), the temperature of freshly mixed concrete containing POFA can be decreased dramatically due to the slow heat of hydration of POFA than OPC, thus slowing down the initial setting time of cement and provide higher slump value to the mixes [25]. Indeed, this lower temperature in the concrete mix (e.g., mass concrete application) could minimize thermal cracking, thus maintaining higher mechanical strength and better durability. On the contrary, highly workable concrete mixes could guarantee better compaction, thus removing the voids from the concrete specimens and reducing the porosity and permeability, leading to higher mechanical strength. This higher sump of POFA concrete mixes is aligned with the mechanical strength of concrete, as discussed in Section 3.2.

As demonstrated in Fig. 7, the density of all mixes (presented at the secondary axis of Fig. 7) decreased due to the introduction of POFA compared to the control OPC mix. In comparison to OPC concrete, 45 % POFA-containing concrete depicted the minimum density (2304 kg/m^3). Additionally, the fall in density lies between 1 % and 6%for all the mixtures. The most significant value was considerably observed for the control mix, considering no replacement of OPC. The obtained result can be correlated with the study of Ortiz et al. [78], who also observed a similar pattern. When more POFA is added to cement paste, the time it takes to set lengthens [79]. Thus, the density also decreased with the time of setting. The decrease in density of concrete fabricated with POFA could be associated with a substantially lower specific gravity of POFA than OPC (2.18 for POFA and 3.15 for OPC). This property will dramatically decrease the self-weight, i.e., the density of concrete, and it is more evident for the higher replacement level of OPC with POFA (e.g., 45 %), as shown in Fig. 7.

3.1.2. Compacting factor

Further considering the consequences, the value of compacting factor increased on the verge of using a proper percentage of POFA. Almost all the proportion of POFA replaced mixtures shows a greater degree of compacting factor, represented at the primary axis of

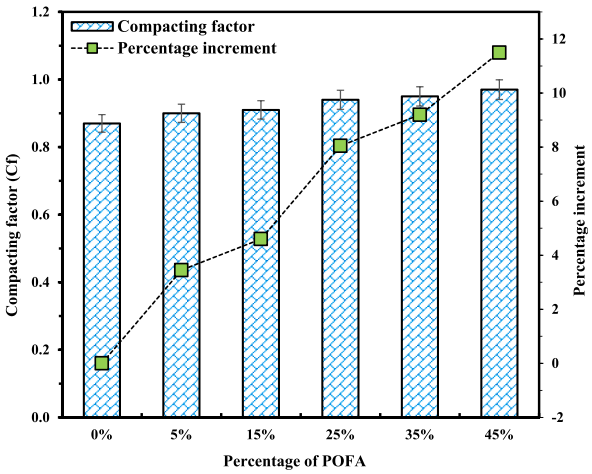

Fig. 8. Average slump and compacting factor test values of concrete mixes.

Fig. 8. The values of compacting factor ranged from 0.87 to 0.97 in every concrete mixture, where the control mix showed a compaction factor of 0.87. The greatest compacting factor was conceded, replacing 45 % OPC with POFA, which was around 11.5 % higher than the control mix. A similar finding of compacting factor test consequences was also considered by Zeyad et al. [32].

Furthermore, the compacting factor (C_f) and slump (S) test results can characterize a linear correlation. Correlations were determined using linear regression analysis. Equation (5-a) represents the relation between the slump test and compacting factor test with 93 % correlative confidence.

$$C_f = 0.0025S + 0.716 \tag{5-a}$$

According to equation (1), a correlation may classify concrete yield stress (f_y) using the slump test results without performing the experimental study. From Fig. 9, the correlation between yield stress and slump values can be characterized, which shows a linear relationship between the yield stress and the slump rate for fresh concrete, where a substantial slump value suggests a low resistance for flowing and a low yield stress is indicated in equation (5-b) with a correlation coefficient of 99 %.

$$f_y = -11.67S + 2873.5 \tag{5-b}$$

3.1.3. Machine learning strategies on fresh characteristics

Experimentation data and predictions for the slump, compacting factor, and yield stress are presented in Figs. 10–12, after being subjected to a regression evaluation using the RF, and ANN models. The substantial correlation coefficients that the specified slump value models effectively attained are exhibited in Fig. 10. The coefficient of regression (R^2) values (shown in Fig. 10) for the RF and ANN approaches used for predicting the slump values are 0.978 and 0.871, respectively. Furthermore, it indicates that RF is superior to ANN in this data set's slump value prediction.

The similarity between observed and predicted values for the compacting factor is similarly highlighted in Fig. 11. Impressive outcomes were observed between the suggested RF and ANN models, with correlation values of 0.987 and 0.911, respectively. Consequently, the ML model's performance in predicting the compacting factor was rated satisfactory using these findings from experiments.

The regression coefficient generated by the ML-driven technique, when used to predict the outcome of yield stress, is outstanding, as shown in Fig. 12. In contrast, the RF and ANN models had similar regression coefficients of about 0.975 and 0.97, respectively. As a result, the suggested models are the most precise for the current research.

3.2. Mechanical performance

3.2.1. Effects of POFA on compressive strength

Obtained test consequences for the compressive strength of all of the mix designs are depicted in Table 4 concerning the variation of statistical parameters such as standard deviation, mean strength, standard error, coefficient of variation (CoV), and the range of 95 % confidence interval between lesser and greater amounts for 7 days, 14 days, and 28 days. Each detail was obtained by considering the mean among three sequentially tested samples. With the replacement of cement by POFA up to 15 %, an upward trend of 28 days of compressive strength could be observed. Replacement of 25 % cement content by POFA maintained significant strength, followed by a strength drop for a higher percentage replacement of OPC with POFA. The drop in strength with more than 25 % replacement could be for the slow hydration process and the delay in the reaction of pozzolana considering the POFA particle.

Fig. 13 illustrates the graphical representation of the strength of compressive of all concrete mixtures. Compressive strength assessment was enhanced and correlated with the control mixture, thanks to the data that illuminated the process of POFA incorporation in concrete. The highest compressive strength was found in mixtures with 15 % cement substitution by POFA. This mixture's

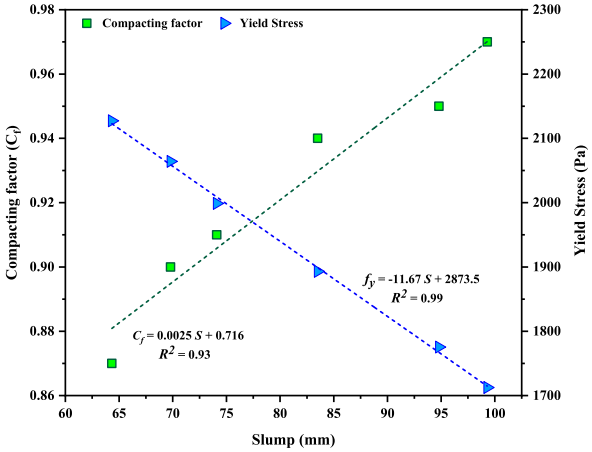

Fig. 9. Relationship of slump with compacting factor and yield stress.

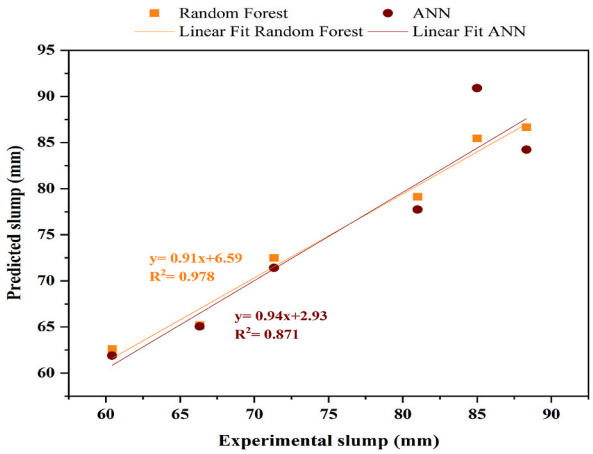

Fig. 10. Regression comparison of actual and predicted slump values.

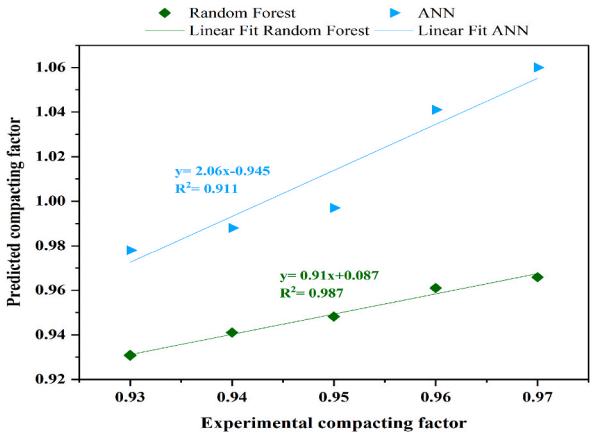

Fig. 11. Regression comparison of actual and predicted compacting factor values.

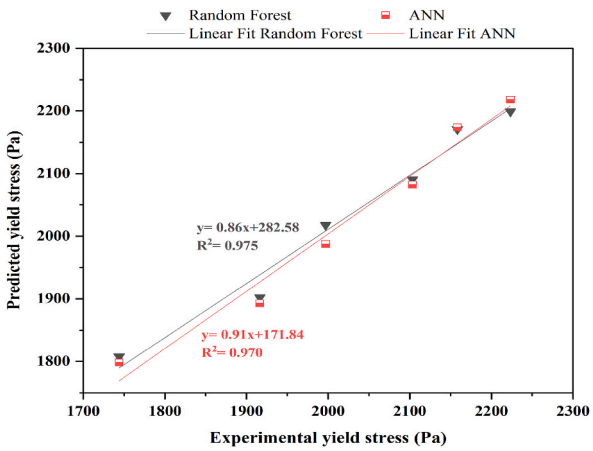

Fig. 12. Regression comparison of actual and predicted yield stress values.

compressive strength is 4.5 % higher than the reference mixture. From Fig. 14, the percentage of increase for compressive strength can be visualized, which indicates the improvement of compressive strength for 5 % and 15 % of POFA replacements.

The augmented compressive strength of concrete fabricated with POFA could be associated with the hydration reaction, micro filler

Table 4
Overview of the POFA replacement mix compressive strength test findings.

Mix	Days	Mean strength (MPa)	Standard deviation	CoV (%)	Standard error	95 % confidence interval	
						Lower range	Upper range
0 % POFA	7	23.030	0.383	0.017	0.221	22.66	23.43
	14	31.104	0.085	0.003	0.049	31.02	31.19
	28	37.037	0.352	0.010	0.203	37.4	36.7
5 % POFA	7	24.363	0.187	0.008	0.108	24.21	24.57
	14	31.456	0.145	0.005	0.084	31.04	31.62
	28	37.552	0.800	0.021	0.462	36.62	38.01
15 % POFA	7	23.455	0.179	0.008	0.104	23.24	23.58
	14	30.787	0.103	0.003	0.059	30.67	30.88
	28	38.799	0.228	0.006	0.132	38.53	38.97
25 % POFA	7	22.891	0.319	0.014	0.184	22.25	22.73
	14	29.989	0.108	0.004	0.062	29.88	30.09
	28	37.067	0.079	0.002	0.046	36.99	37.16
35 % POFA	7	12.757	0.188	0.015	0.109	12.54	12.91
	14	19.979	0.134	0.007	0.077	19.84	20.11
	28	23.549	0.630	0.027	0.364	23.09	24.27
45 % POFA	7	8.044	0.722	0.090	0.417	7.21	8.53
	14	12.643	0.238	0.019	0.138	12.43	12.9
	28	16.864	0.445	0.026	0.257	16.4	17.3

effects, and the pozzolanic response of the high fineness of POFA [80]. The reaction between POFA and calcium hydroxide ($Ca(OH)_2$) initiates a pozzolanic reaction, resulting in the formation of secondary calcium-silicate-hydrate (C–S–H) [25]. This reaction contributes to the compaction of the concrete microstructure, ultimately leading to increased strength. For the early age condition, the hydration response of OPC governs the strength advancement of the control concrete. Conversely, the development of strength in the concrete mixes with POFA and OPC is associated with the hydration reaction of OPC and the packing effect. As shown in Fig. 3b, the POFA particles are significantly higher fineness and smaller than OPC particles, which can fill the microvoids among cement particles and the aggregates [23]. This phenomenon dramatically reduces the porosity and pore connectivity (i.e., lower permeability) in the matrix, significantly refines the concrete's microstructure, and augments the compressive strength of concrete. At a later age, the enhancement in compressive strength of concrete mixes containing POFA could occur in two stages: (i) First, the strength development is due to the hydrated product of OPC (e.g., calcium silicate hydrate-CSH and calcium hydroxide-CH), which is occurred in control mix and mixes with POFA. (ii) in the second stage, secondary C–S–H gels formed due to the pozzolanic activity of POFA, which is missing in the control mix and makes a difference in the strength development [22]. As reported in Fig. 3b, the POFA has a higher fineness and sufficient specific surface area to undergo greater pozzolanic reaction, as occurred for the other pozzolanic materials, such as fly ash. Also, POFA will fill the voids in the concrete matrix. As shown in Fig. 4 and Table 1, POFA has a significantly higher content of SiO_2, which can react with the hydration clinker compounds (CH) in the presence of water regarding the concrete's material. These characteristics could form secondary CSH gels, thus significantly reducing the matrix's porosity and permeability, providing dense microstructure, and boosting the interaction among the paste of cement and aggregates. These properties improve the mechanical strength of the concrete mixes fabricated with POFA.

On the other hand, the decrement in the compressive strength is observed in the 35 % POFA and 45 % POFA mixes. The decrease in

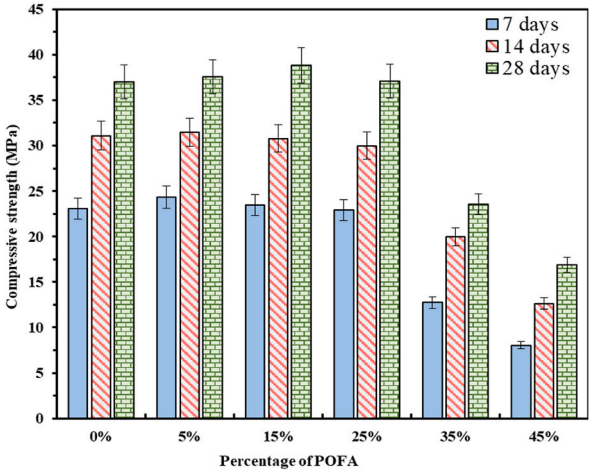

Fig. 13. Compressive strength at 7,14, and 28 days.

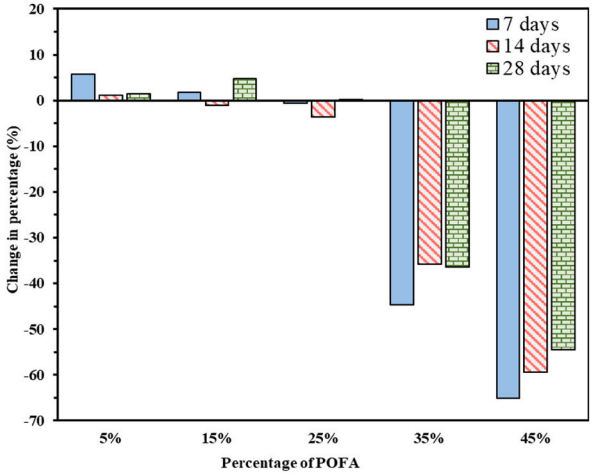

Fig. 14. Fluctuation of compressive strength compared with the reference mix.

CH produced by cement hydration may cause the decreased pozzolanic reaction in high-replacement cement made using POFA. As a result, POFA mixes had lower compressive strengths than concrete with a low POFA component. Sata et al. [81], and Alsubari et al. [45] also found a similar pattern; in their study, a 20 % replacement of POFA showed an optimum result. However, 25 %, 35 %, and 45 % substitution of cement by POFA describe a huge decrement in compressive strength. The slow hydration process and the delay in the pozzolanic reaction of POFA particles could be a reason for the strength decrement [25].

3.2.1.1. Machine learning strategies for compressive strength. A boxplot of the predicted and experimental relationship is presented in Fig. 15. Boxplots, which summarise data employing five variables (the "minimum," "first quartile," "median," "third quartile," and "maximum"), are often used to display statistical distributions of data. Statistics such as the mean, median, interquartile range, least, and peak are presented in these investigations of individuals. The median margins for every data set appeared inside the relevant boxes, indicating that there was probably not much difference across the various groups.The variability of this set of results was not exceedingly wide when expressed by the interquartile range or box length. Furthermore, the presented models like RF, ANN and their ensemble had no unexpected results. Even though most data only goes as far back as 28 days, knowing how POFA develops its strength over time is essential for using it as a pozzolanic material in buildings. To overcome this shortcoming and shed light on the long-term strength properties of POFA-based concrete, machine learning approaches like RF and ANNs provide a viable path. Modelling the connection between POFA concentration, curing conditions, and final concrete strength is possible because to RF's capacity to capture complicated interactions between components. In addition, ANNs, which are adept at interpreting non-linear patterns, may use what they have learned from past data trends to project the strength growth beyond the 28-day mark. These ML techniques allow scientists to more accurately foretell the long-term strength of POFA-based concrete, which improves the mix design and guarantees the long-

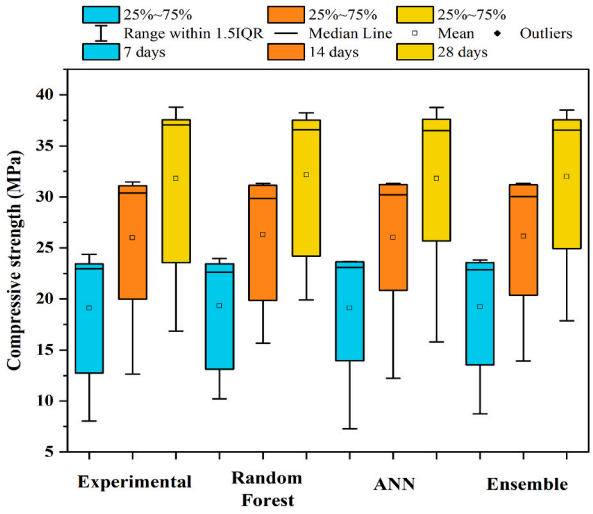

Fig. 15. Box plot illustrating the range of compressive strength values.

term stability of buildings built with this eco-friendly material. In addition, the knowledge gathered from these ML methods may eventually lead to greener and more efficient building methods.

Fig. 16 demonstrates that compared to experimental results, both the RF and ANN strategies provide reliable predictions. The linear relationship coefficient was 0.988 in the RF model, 0.991 in the ANN model, and 0.996 in the ensemble models. The MAE, MSE, and RMSE for the ANN model were 0.73, 1.13, and 1.06, while the RF model was 0.96, 1.93, and 1.39; however, the ensemble model produced values of 0.66, 0.72, and 0.85. This indicates that the ensemble model is quite good at making predictions.

3.2.2. *Effects of POFA on splitting tensile strength*

Table 5 shows the splitting tensile strength of all the mixtures concerning various parameters considering statistics such as CoV, mean strength, standard error, standard deviation, and the lesser and greater range of 95 % confidence boundary for 7 days, 14 days, and 28 days, respectively. All the details were obtained from the mean among three sequentially tested samples. It is experienced from the laboratory data that the strength of tensile in all POFA mixes was within the variation of 0.74 MPa–2.05 MPa at 7 days, while for 14 days, the strength increased to a range of 0.96 MPa–2.16 MPa, and for 28 days the strength increased to a range of 1.16 MPa–2.28 MPa. The test results of the specimen of a particular day deviated from 0.006 to 0.012. On the contrary, the corresponding CoV is 0.001 %–0.02 %.

Fig. 17 represents the strength of splitting tensile for all the concrete mixes, which depicted an increment of tensile strength of concrete mixes fabricated with 5 %,15 %, and 25 % POFA than the control mix. However, the decreased pattern of splitting tensile strength concerning POFA replacement is similar to the compressive strength value. The percentage increment and decrement of strength considering tensile values are presented in Fig. 18. The observation implies almost a 36 % increase in tensile strength for concrete, where 15 % of cement had been replaced by POFA compared to the control mix (0 % POFA) at the curing period of 28 days. On the contrary, the value differs more than 50 % downwards for 45 % of POFA replacement at 28 days.

POFA acts as a filler and produces supplementary C–S–H to boost the binding capacity of concrete when added to the matrix [82]. However, the mechanism for enhancing the tensile strength of concrete mixes containing POFA should be similar, as discussed in Section 3.2.1. Previous research have also indicated that POFA concrete exhibits a notable propensity for self-healing, resulting in reduced permeability and enhanced durability [30]. Tambe and Nemade [83] also observed a comparable pattern of variability in tensile strength. Also, the studies of Mohammadhosseini et al. [84] and Alsubari et al. [43] stated that the increment of tensile strength ranges from 7 % to 30 % replacement of POFA in self-consolidating concrete. Nevertheless, a reduction in the tensile strength was noticed for concrete containing 30 % and 60 % substitution of cement with POFA by renowned authors like Siddique [85] and Nikbin et al. [86].

3.2.2.1. Machine learning strategies for splitting tensile strength. A box plot depicts the splitting tensile strength, as shown in Fig. 19, in an approach identical to the one used to demonstrate the statistical distribution for compressive strength. These strength data showed slight fluctuation; the interquartile ranges were 0.38 MPa–1.92 MPa after 7 days, 0.60 MPa–1.51 MPa after 14 days, and 1.16 MPa–2.94 MPa after 28 days. The median lines for all sets of data were all encompassed inside the corresponding boxes, indicating that there was likewise minimal variation across the groups. The strength forecasts made using these methods go much beyond the standard 28-day data. To make more precise strength forecasts, ANNs can handle non-linear patterns, whereas RF excels at capturing complicated correlations. Because of this, mix designs may be optimized and the endurance of sustainable materials can be guaranteed, leading to more efficient and environmentally responsible construction.

The precision of projections given by both the RF and ANN approaches is shown in Fig. 20 by comparison with experimental findings. The coefficient for linearity in the RF model was 0.993, the ANN model was 0.916, and the ensemble models were 0.979. Regarding predictive accuracy, RF and the ensemble models outperform ANN because of an improved correlation coefficient. The

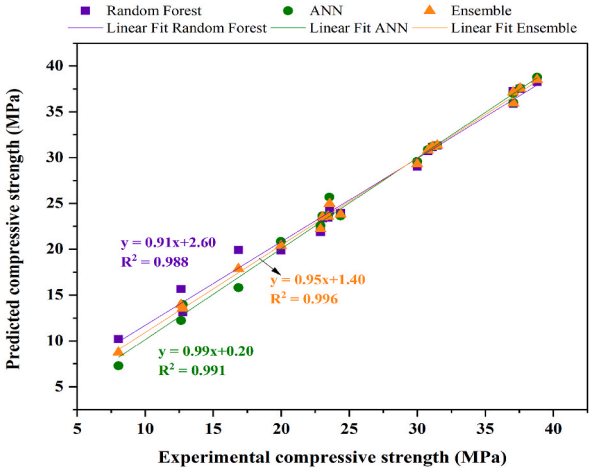

Fig. 16. Relationship between predicted and experimental results of compressive strength.

Table 5
Overview of the POFA replacement mix splitting tensile strength test findings.

Mix	Days	Mean strength (MPa)	Standard deviation	CoV (%)	Standard error	95 % confidence interval	
						Lower range	Upper range
0 % POFA	7	1.470	0.013	0.009	0.007	1.36	1.59
	14	1.630	0.021	0.013	0.012	1.52	1.75
	28	2.100	0.019	0.009	0.011	1.99	2.22
5 % POFA	7	1.820	0.002	0.001	0.001	1.71	1.94
	14	1.960	0.018	0.009	0.010	1.85	2.08
	28	2.450	0.011	0.005	0.006	2.34	2.57
15 % POFA	7	2.050	0.006	0.003	0.003	1.94	2.17
	14	2.160	0.012	0.006	0.007	2.05	2.28
	28	2.860	0.010	0.004	0.006	2.75	2.98
25 % POFA	7	1.780	0.036	0.020	0.021	1.67	1.9
	14	1.900	0.020	0.011	0.012	1.79	2.02
	28	2.570	0.015	0.006	0.009	2.46	2.69
35 % POFA	7	1.430	0.012	0.009	0.007	1.32	1.55
	14	1.680	0.008	0.005	0.005	1.57	1.8
	28	1.960	0.012	0.006	0.007	1.85	2.08
45 % POFA	7	0.740	0.007	0.009	0.004	0.63	0.86
	14	0.960	0.004	0.004	0.002	0.85	1.08
	28	1.160	0.006	0.005	0.004	1.05	1.28

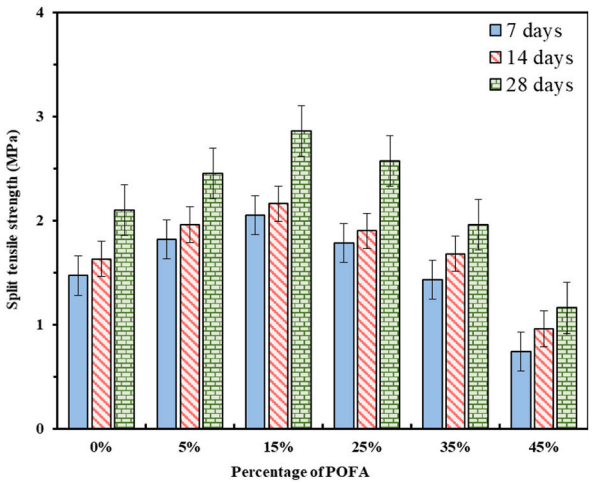

Fig. 17. Evaluated splitting tensile strength at 7,14, and 28 days.

MAE, MSE, and RMSE for the RF model were respectively 0.11, 0.022, and 0.149, while for the ANN model, the results were respectively 0.59, 0.13, and 0.47; nevertheless, the ensemble model generated values of 0.32, 0.052, and 0.29.

3.2.3. Splitting tensile strength vs. compressive strength

Fig. 21 shows a scatter pattern depicting the association between compressive strength and splitting tensile. Linear projections of the POFA replacement regression model are presented in equation (6) and depicted graphically in Fig. 21. These relationships can explain approximately 81 % of variability, as measured by their R^2 coefficient of determination.

$$f_{st} = 0.0583 f_c + 0.3274 \tag{6}$$

Where f_{st} = mean splitting tensile strength, f_c = mean compressive strength.

In Fig. 21, the confidence intervals were calculated for equation (6), and scattering was plotted. These laboratory values of the splitting tensile strength were also compared with the calculated strengths of various standards illustrated in Fig. 19. The AS 3600 (AS 2009) [87], ACI 363 R [88], ACI 318 (ACI 2008) [89], and CEB-FIP (1992) [90] give models [equations (7)–(10)] to illustrate the graphical and equational relationship among the strength of splitting tensile and compressive.

$$f_{st} = 0.4\sqrt{f_c}\,(AS3600) \tag{7}$$

$$f_{st} = 0.59\sqrt{f_c}\,(ACI363R) \tag{8}$$

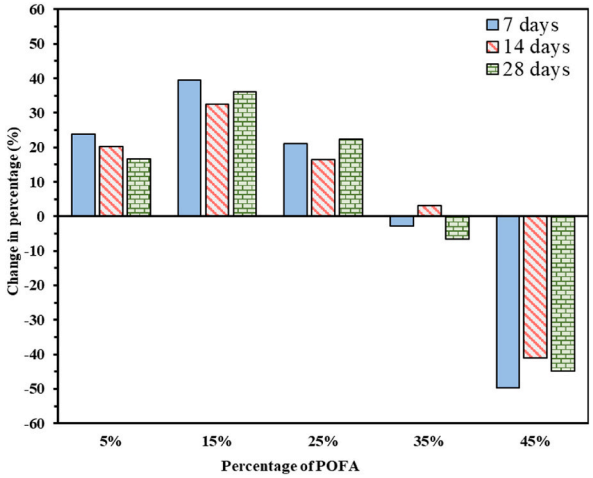

Fig. 18. Fluctuation of splitting tensile strength compared to the control mix.

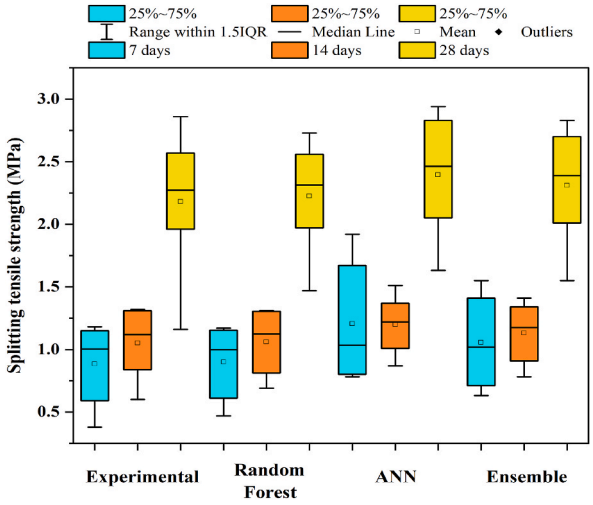

Fig. 19. Box plot illustrating the range of splitting tensile strength values.

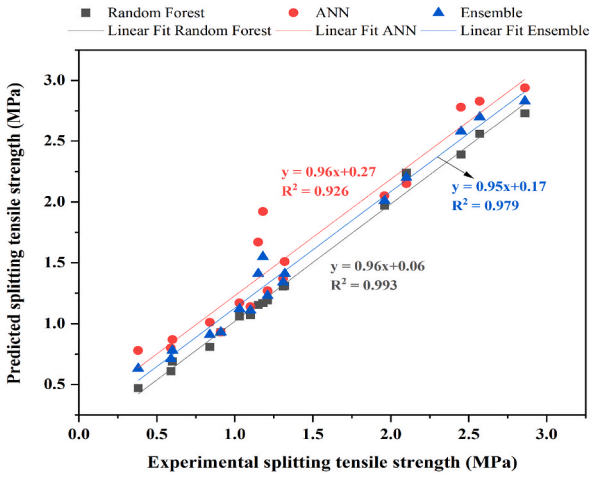

Fig. 20. Relationship between predicted and experimental results of splitting tensile strength.

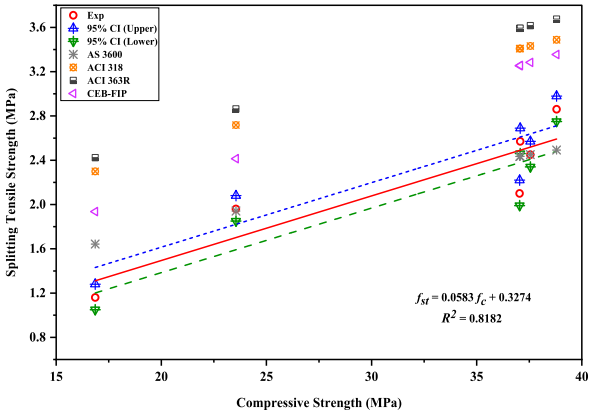

Fig. 21. Relation between splitting tensile strength and compressive strength.

$$f_{st} = 0.56\sqrt{f_c}(ACI318) \tag{9}$$

$$f_{st} = 0.3(fc)^{2/3}(CEB - FIP) \tag{10}$$

According to the linear correlation model, it is obtained that only AS 3600 (AS 2009) standards lie within the upper confidence interval and lower confidence interval. Therefore, the values were near to the experimental values of this experiment, and a scatter pattern was observed for ACI 363 R (ACI 1992), ACI 318 (ACI 2008), and CEB-FIP (1992).

3.2.4. *Effects of POFA on flexural strength*

In Table 6, various statistical parameters are depicted and calculated from flexural strength values at 7 days, 14 days, and 28 days. It is detected from the data that flexural strength increased up to 25 % of POFA replacement at 7 days, 14 days, and 28 days. The lowest strength value was recorded at 1.21 MPa for 45 % POFA at 7 days; the corresponding CoV and standard error values are 0.0058 % and 0.0040, respectively. Similarly, the maximum strength value was recorded as 5.26 MPa for 15 % POFA at 28 days, and the corresponding CoV and standard error values are 0.0020 % and 0.0060, respectively. The test results deviated from one specimen to another and were noted from a minimum of 0.0021 to a maximum of 0.0362.

From Fig. 22, an increment of flexural strength can also be visualized for 5 %,15 %, and 25 % replacement of POFA. This increment may be attributable to the refinement of microstructure caused by the production of extra CSH gels by the pozzolanic reaction of the reactive silica in POFA [91]. After further addition of POFA, the decrement of flexural strength maintains an equivalent trend compared to the compressive as well as tensile strength values. The percentage increment and decrement of flexural strength values are presented in Fig. 23. There was almost a 31 % increase in flexural strength for 15 % POFA incorporated concrete mix compared to the reference mix at 28 days. However, the value differs more than 50 % downwards for 45 % POFA replacement. The lower percentage of CaO and the slower reaction characteristics of POFA (i.e., a highly porous matrix that could cause stress concentration and weaken the bond between cement paste and aggregates) could be a reason for strength decrement when mixed at a higher volume.

The experimental value can also be justified by previous studies such asMohammadhosseini et al. [84] and Ranjbar et al. [92]. The additional silica in POFA can interact with portlandite and produce secondary CSH gel. The extra CSH gel was created due to the POFA's pozzolanic response, which was dependent on the formation of portlandite. The study of Ranjbar et al. [92] states the highest flexural strength gained for 15 % of cement replacement by POFA of self-compacting concrete. However, adding POFA in high concentration decreased flexural strength when compared with concrete samples that did not contain POFA.

3.2.4.1. Machine learning strategies of flexural strength. Fig. 24 portrays boxplots of flexural strength data from experiments and predictions. Numerous statistical indicators, including the mean, the standard deviation, the median, the interquartile range, the least, and the peak, are shown. None of the models had extremely erroneous distributions of predicted and experimental findings. The fact that all median lines fell within the associated boxes suggests that there was seemingly little difference across the datasets. The results were not evenly spread as seen by an interquartile range of 1.49–5.11 MPa at 7, 14, and 28 days. ML may extrapolate over this time period, which is normally limited to 28 days due to data restrictions. For more precise forecasts of long-term strength, ANNs are preferable to Random Forest because of their superiority in modeling non-linear patterns.

Fig. 25 shows that when contrasted with experimental results, the RF and ANN techniques provide precise projections. A linear relationship was estimated to be 0.989 in the RF model, 0.972 in the ANN model, and 0.985 in the ensemble models. With a higher correlation coefficient, RF and the ensemble models are superior to ANN using precision in prediction. The RF model delivered the best outcomes with values of 0.15, 0.03, and 0.18 for MAE, MSE, and RMSE, respectively. The RF model performed more effectively with lower MAE, MSE, and RMSE values than the ANN model.

Table 6
Overview of the POFA replacement mix flexural strength test findings.

Mix	Days	Mean strength (MPa)	Standard deviation	CoV (%)	Standard error	95 % confidence interval	
						Lower range	Upper range
0 % POFA	7	2.33	0.0128	0.0055	0.0074	2.22	2.45
	14	3.3	0.0206	0.0062	0.0119	3.19	3.42
	28	4.02	0.0192	0.0048	0.0111	3.88	4.16
5 % POFA	7	2.66	0.0021	0.0008	0.0012	2.55	2.78
	14	3.73	0.0180	0.0048	0.0104	3.62	3.85
	28	4.61	0.0110	0.0024	0.0064	4.47	4.75
15 % POFA	7	2.91	0.0055	0.0019	0.0032	2.8	3.03
	14	3.77	0.0123	0.0033	0.0071	3.66	3.89
	28	5.26	0.0103	0.0020	0.0060	5.12	5.4
25 % POFA	7	2.65	0.0362	0.0137	0.0209	2.54	2.77
	14	3.39	0.0204	0.0060	0.0118	3.28	3.51
	28	4.55	0.0153	0.0034	0.0088	4.41	4.69
35 % POFA	7	2.05	0.0124	0.0061	0.0072	1.94	2.17
	14	2.37	0.0084	0.0035	0.0049	2.26	2.49
	28	2.87	0.0120	0.0042	0.0069	2.73	3.01
45 % POFA	7	1.21	0.0070	0.0058	0.0040	1.1	1.33
	14	1.48	0.0041	0.0028	0.0024	1.37	1.6
	28	1.91	0.0064	0.0033	0.0037	1.77	2.05

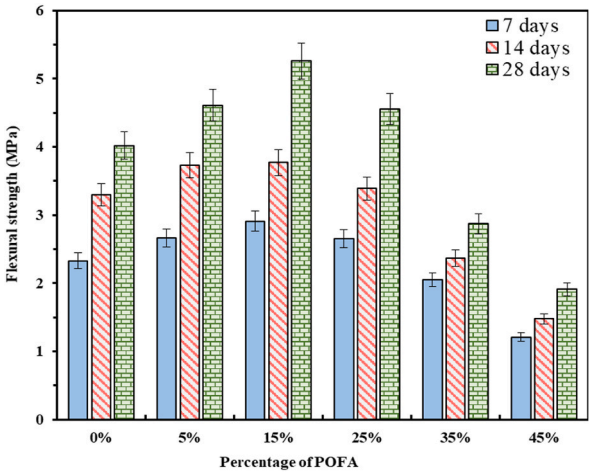

Fig. 22. Flexural strength at 7,14, and 28 days.

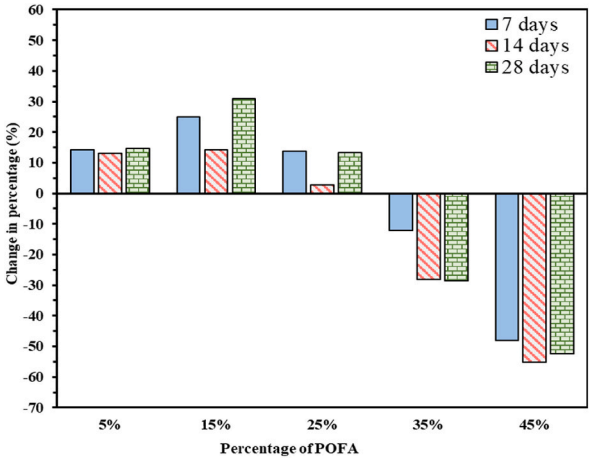

Fig. 23. Fluctuation of flexural strength compared to the control mix.

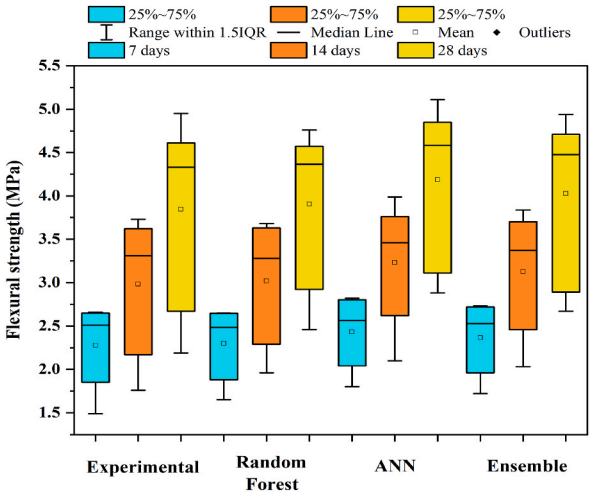

Fig. 24. Box plot illustrating the range of flexural strength values.

3.2.5. *Flexural strength vs compressive strength*

Fig. 24 illustrates the association between flexural strength and compressive strength in a linear graph. The anticipated regression approach for POFA replacement is shown through the linear trajectory in Fig. 26 and shown in Equation (11). The coefficient of determination R^2 of these relations is found to be 93 %, which indicates a very strong correlation.

$$f_{fr} = 0.1304 f_c + 0.2784 \tag{11}$$

where, f_{fr} = mean flexural strength, f_c = mean compressive strength.

Confidence intervals were estimated and projected in Fig. 24**.** These testing flexural strength readings were additionally contrasted to the estimated strengths of different standards, as illustrated in Fig. 24. The AS 3600 (AS 2009) [87], ACI 363 R [88] and ACI 318 (ACI 2008) [89], and CEB-FIP (1992) [90] give models [equation (12)–(15)] to represent the relationship among flexural and compressive strength.

$$f_{st} = 0.4\sqrt{f_c}(AS3600) \tag{12}$$

$$f_{st} = 0.59\sqrt{f_c}(ACI363R) \tag{13}$$

$$f_{st} = 0.4\sqrt{f_c} f_{st} = 0.56\sqrt{f_c}(ACI318) \tag{14}$$

$$f_{st} = 0.3(fc)^{2/3}(CEB - FIP) \tag{15}$$

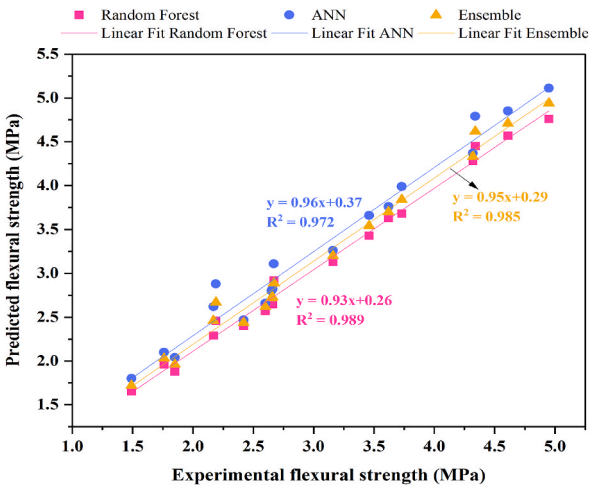

Fig. 25. Relationship between predicted and experimental results of flexural strength.

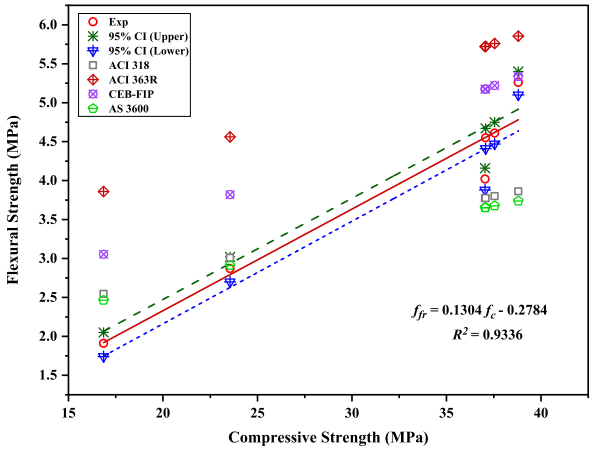

Fig. 26. Relation between flexural strength and compressive strength.

The linear regression model shows that AS 3600 (AS 2009) and ACI 318 (ACI 2008) standards lie within the upper and lower confidence interval. For these two cases, the values were near to the experimental values of this experiment. However, a little scatter was observed for CEB-FIP (1992) and ACI 363R (ACI 1992).

3.3. Microstructural analysis

Fig. 27a depicts the SEM images of the control mix with containing 0 % POFA whereas the optimum mix including 15 % POFA is shown in Fig. 27a. The microstructures of the concrete specimens show significant variances when compared to one another. Large pores and smaller pores that were less evenly spread were visible in the microstructures of the control mixture, thus implying higher porosity and permeability. Contrastingly. a more uniform structure was achieved as the concentration of POFA grew; also, an increase in POFA resulted in a more excellent formation of CSH gels [35]. After 28 days, a higher strength growth can be attributed to the POFA specimens that had reduced micropores. Because the fine particles of POFA could occupy the specimens' micropores, the density of the mixture increased, which led to an increase in mechanical strength. The enhanced microstructure of the cement paste including POFA can be assigned to the augmented formation of C–S–H gel resulting from the hydration process and the pozzolanic interaction between POFA and $Ca(OH)_2$, as reported by Zeyad et al. [34]. Overall, the presence of these supplementary gels can lead to enhanced microstructural characteristics, resulting in greater density of concrete and improved resistance against degradation mechanisms such as chloride, carbonation, sulphate, and acid attack [35].

3.4. Sustainability assessment

3.4.1. eCO_2 analysis

Cement production results in about 3.3 gigatons of CO_2 emissions worldwide every year [93]. Thus, replacing OPC with waste leads to developing sustainable and environmentally friendly concrete and minimizes greenhouse gas emissions [94]. For this, the cradle-to-gate approach was incorporated to evaluate the total energy for concrete material mining, transportation, and preparation [95]. The total eCO_2 released for material transportation was also computed as presented in Table 7, which also shows the appropriate references for each item. The total eCO_2 emission of the material was calculated by adding the eCO_2 emissions from production and the

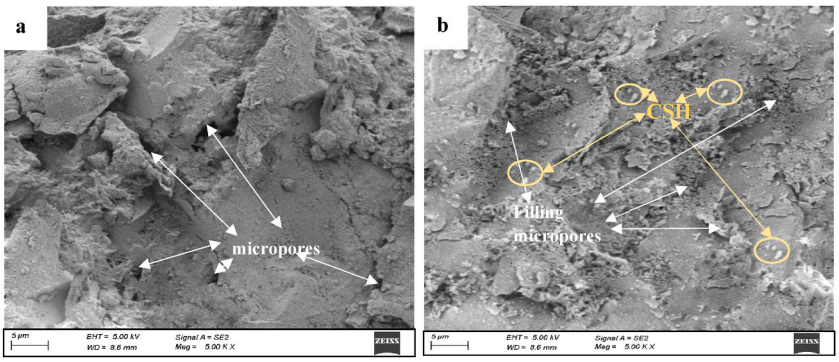

Fig. 27. SEM images of the (a) 0 % POFA and (b) 15 % POFA specimens.

eCO_2 emissions from transportation. Fig. 28 shows the estimated eCO_2 and cement replacement rate connection. When POFA replaces cement, eCO_2 emissions are significantly reduced. The eCO_2 of 5 % POFA, 15 % POFA, 25 % POFA, 35 % POFA, and 45 % POFA concrete mixes achieve 95.10 %, 85.31 %, 75.51 %, 65.72 %, and 55.92 %, respectively of 0 % POFA which consisting of only cement as binding material. As a result, POFA concrete mixes can achieve 44.08 % eCO_2 reduction due to a 45 % substitution of cement. However, Celik et al. [93] reported that 50 % fly ash replacement of cement reduces eCO_2 emissions by around 47 %, whereas a combination of 60 % fly ash and 15 % limestone powder reduces 67 % eCO_2 emissions. Therefore, industrial waste bi-product POFA can achieve environmental sustainability by reducing embodied CO_2 and embodied energy emissions of the concrete mixes.

3.4.2. Cost analysis

The concrete cost is an important issue to consider during the manufacturing of the mixes. In this study, the cost of key materials for preparing POFA mixes is shown in Table 7. However, it is observed that OPC costs 9.8, 8.8, and 2.32 times higher than coarse aggregate, sand, and POFA, respectively. As a result, cement is the primary cost factor in concrete. As illustrated in Fig. 29, it was obtained that replacing cement with POFA reduced concrete costs per m^3. In addition, 5 %, 15 %, 25 %, 35 %, and 45 % of the POFA mix saved 0.5 %, 1.1 %, 2.52 %, 3.53 %, and 4.54 % cost, respectively, compared with the 0 % POFA mix. It is also obtained that using a high-volume POFA mix cuts concrete costs significantly. Beyond manufacturing an economical concrete mix, using this POFA waste as cement replacement increases mechanical characteristics while reducing environmental risks.

3.4.3. Case study of a G+7 storied residential structure

An eight-story residential construction plan, as shown in Fig. 30, was used to demonstrate real-world projects' financial viability and carbon emission. The costs and eCO_2 emissions for the beams, columns, and slabs were computed independently to have a more comprehensive knowledge of the POFA's economic and environmental effects on structural components, as shown in Table 8. This method made it possible to analyze each structural component in greater depth, giving vital information about the viability and prospective uses of the current data. It can be simple to spot opportunities for cost savings and places where changes could be made to lessen the project's environmental impact.

Table 8 shows the analytical cost and eCO_2 emission for slab, beam, and column members for the incorporation of 0 %–45 % POFA used as a cement substitute in the mixture of concrete. Additionally, the summation of all these members is graphically presented in Fig. 31, which depicts that the total cost using conventional concrete (0 % POFA) was 344 thousand MR. The total cost was decreased to 324 thousand MR with the substitution of 45 % cement with POFA, which represents a decrease of about 6 % in the concrete cost. On the other hand, when all the members were combined, the eCO_2 emission likewise fell from 277 thousand kg to 214 thousand kg in the case of 45 % cement replacement. As compared to conventional concrete that did not contain POFA, this reduction was about 23 %. According to the findings, the utilization of POFA has the promise of helping substantially reduce the carbon emissions associated with the construction industry.

4. Conclusions and recommendations

This study investigated the addition of POFA as a cementitious material, and based on the findings of the study, the following conclusions can be drawn.

- In general, POFA as a waste material demonstrated considerable promise for usage as a replacement for OPC while maintaining acceptable levels of fresh and mechanical qualities.
- The increasing concentration of POFA exhibits a gradual increment of concrete workability and compaction for every mix, with a maximum increment of 54.36 % in a slump and 11.5 % in a compacting factor.
- The addition of POFA showed improved mechanical properties for certain replacement percentages. As 15 % POFA replaced OPC, it depicted the maximum compressive strength, about 38.799 MPa at 28 days curing period.
- Based on the test results, the splitting tensile as well as flexural strength is slightly higher with 15 % POFA replacement compared to the control mix, as the maximum splitting tensile strength of 2.860 MPa and flexural strength of 5.26 MPa was augmented by the concrete mix having 15 % POFA after 28 days of curing period.
- Findings from the ML prediction, it can be seen that RF, ANN, and their ensemble models are superior in predicting fresh and mechanical properties of POFA concrete. These models may be employed for forecasting the strength of concrete that can save time, labour and material costs and ignore to use of heavy machinery.

Table 7
Total eCO_2 emissions and cost at the transportation stage and production stage.

Item	eCO_2 emission (kg CO_2/kg)	Cost (RM/kg)	References
Coarse aggregate	0.005	0.052	[96]
Cement	0.95	0.51	[96]
Water	0.00155	0.008	[97]
Admixture	0.0022	44	[96]
Fine aggregate	0.0048(3)	0.058	[98]
POFA	0.0023(4)	0.22	[43]
Distance (Transportation)	0.18(5)	–	[99]

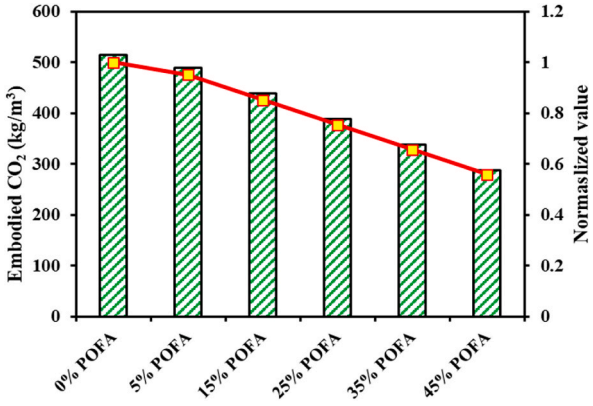

Fig. 28. Embodied CO_2 of the POFA mixes.

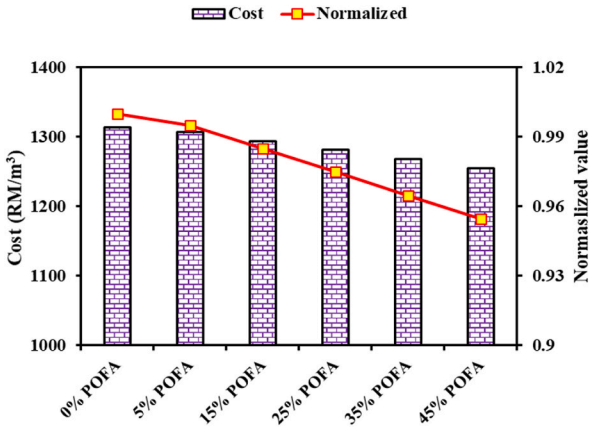

Fig. 29. Cost of POFA concrete mixes.

- The linear regression model using compressive strength test data versus flexural strength and splitting tensile strength displayed a very good co-relation based on R^2 value greater than 0.8 in both cases. A reasonably well prediction can be achieved from the analytical estimation.
- This analytical prediction will be impactful for the future refinement of POFA as a cement replacement. This projected linear regression model may reduce the cost of experimentation by allowing the full exploitation of POFA.
- From the microstructural analysis, it is clear that the finer particles of the POFA fill the micropores in the concrete made with OPC, which leads to improved mechanical performance.
- Finally, the environmental assessment concluded that the POFA mixes reduced up to 4.90 %–44.08 % of eCO_2 emission for 0%–45 % POFA as replacement of OPC. Also, the application of POFA saved the cost of concrete between 0.5 %–4.54 % compared to concrete produced only using OPC. This may be a huge consideration in cement production criteria and reducing carbon footprints to some extent.

This study highlighted the significant advantages of utilizing 15 % by weight of Palm Oil Fuel Ash (POFA) as a cement substitute in concrete mixtures. This optimized POFA concentration not only enhanced concrete's engineering properties but also provided a sustainable and cost-effective solution. The integration of machine learning methods in this research demonstrated promising accuracy in predicting the fresh and mechanical properties of POFA-incorporated concrete. In order to further advance the practicality and applicability of these findings, it is recommended that future research endeavors explore alternative predictive models. Additionally, investigations on the long-term durability of POFA-treated concrete are indispensable, given its pozzolanic properties. Future researches focusing on the corrosion resistance, performance in diverse environmental conditions, and overall structural longevity of this proposed technology is recommended. In conclusion, the findings presented in this study lay a strong foundation for sustainable and cost-effective concrete production through the integration of POFA. However, the pursuit of alternative predictive models and a comprehensive exploration of long-term durability are essential avenues for further research to maximize the benefits and applicability of POFA in concrete engineering.

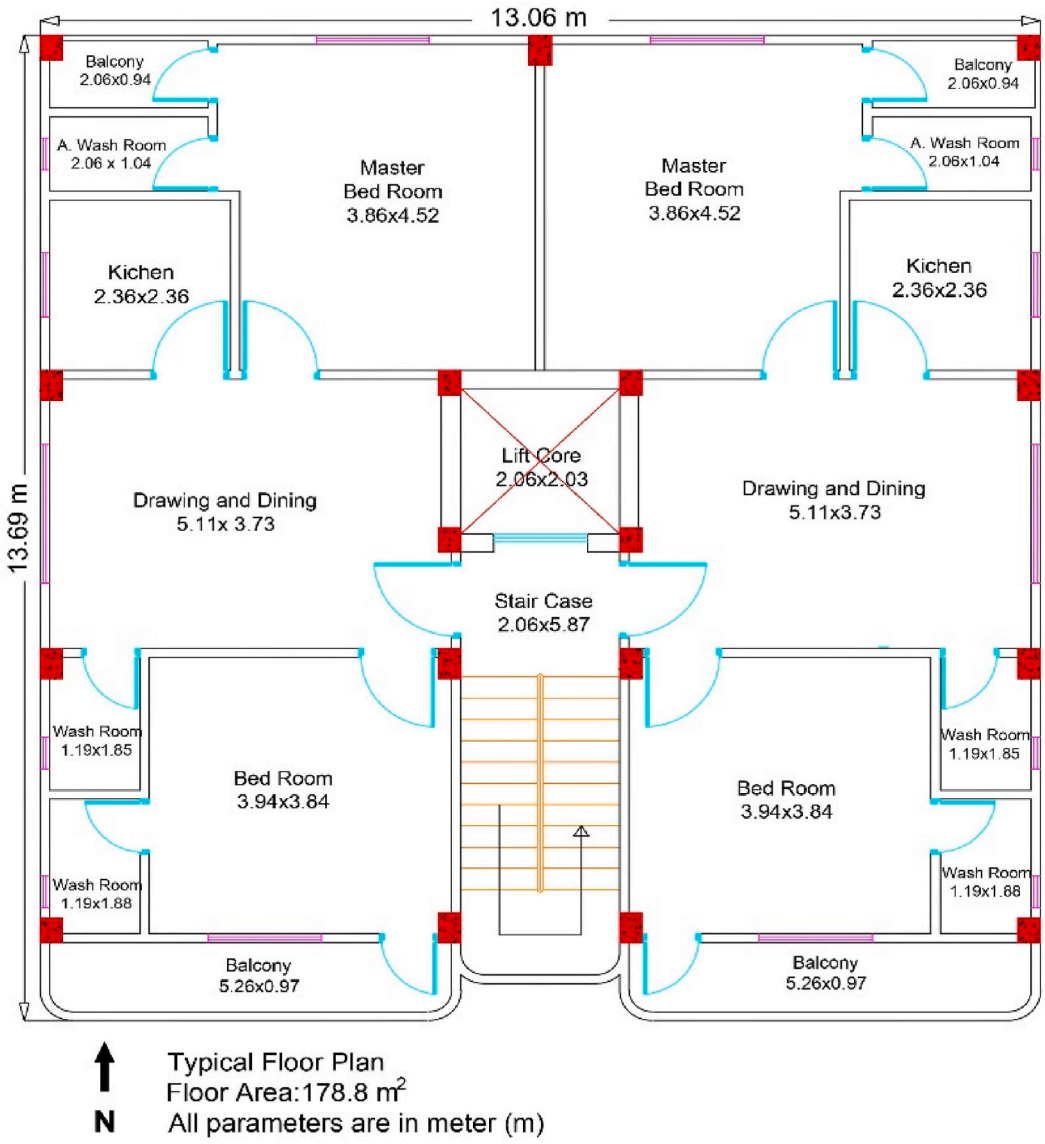

Fig. 30. Typical floor plan of an eight-storied residential building.

Table 8
Costs and eCO_2 emissions of structural members (slab, beam, and column).

Mix id	Cost Breakdown (RM)			eCO_2 Emissions Breakdown (kg CO_2)		
	Slab	Beam	Column	Slab	Beam	Column
0 % POFA	180424	91001	72682	145426	73349	58584
5 % POFA	179300	90435	72230	141754	71497	57104
15 % POFA	177053	89301	71324	134410	67793	54146
25 % POFA	174806	88168	70419	127067	64090	51188
35 % POFA	172558	87034	69514	119723	60385	48229
45 % POFA	170311	85901	68608	112379	56681	45271

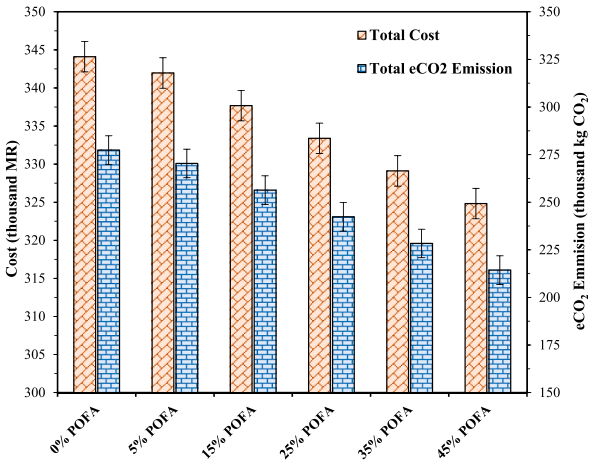

Fig. 31. Total cost and eCO_2 emission of structural members (slab, beam, and column).

Ethical approval

Human subjects are not involved in the study and hence it is not applicable.

Funding statement

This research does not received any external funding.

Data availability

The datasets generated during and/or analyzed during the current study are available from the corresponding author upon reasonable request.

Additional information

No additional information is available for this paper.

CRediT authorship contribution statement

Noor Md. Sadiqul Hasan: Writing – review & editing, Writing – original draft, Validation, Supervision, Methodology, Investigation, Formal analysis, Data curation, Conceptualization. **Md. Habibur Rahman Sobuz:** Writing – review & editing, Writing – original draft, Validation, Supervision, Methodology, Data curation, Conceptualization. **Nur Mohammad Nazmus Shaurdho:** Writing – review & editing, Validation, Formal analysis, Data curation. **Md. Montaseer Meraz:** Writing – review & editing, Writing – original draft, Investigation, Formal analysis. **Shuvo Dip Datta:** Writing – review & editing, Formal analysis, Data curation. **Fahim Shahriyar Aditto:** Writing – review & editing, Formal analysis. **Md. Kawsarul Islam Kabbo:** Writing – review & editing, Formal analysis. **Md. Jihad Miah:** Writing – review & editing, Investigation.

Declaration of competing interest

The authors declare that they have no known competing financial interests or personal relationships that could have appeared to influence the work reported in this paper.

Acknowledgement

The authors would like to be grateful with the laboratory technicians for providing assistance in specimen assembling and testing. The fresh and hardened concrete analysis performed in this paper was carried out at the laboratory of Bandar Universiti Terknologi Legenda Malaysia (University of East London Malaysia Branch). The sustainable analysis of the paper conducted with the high-speed computer in BIM laboratory in the Department of Building Engineering and Construction Management, Khulna University of Engineering and Technology, Khulna – 9203, Bangladesh. The authors would like to show gratitude to the laboratory assistant of the BIM laboratory and other associates for supporting during sustainable, cost analysis and machine learning analysis.

References

[1] X. He, et al., Mine tailings-based geopolymers: a comprehensive review, Ceram. Int. 48 (17) (2022) 24192–24212, https://doi.org/10.1016/j.ceramint.2022.05.345, 2022/09/01/.

[2] N.M.S. Hasan, et al., Rheological, mechanical, and micro-structural property assessment of eco-friendly concrete reinforced with waste areca nut husk fiber, Sustainability 15 (19) (2023), 14131 [Online]. Available: https://www.mdpi.com/2071-1050/15/19/14131.

[3] M. Alyami, I.Y. Hakeem, M. Amin, A.M. Zeyad, B.A. Tayeh, I.S. Agwa, Effect of agricultural olive, rice husk and sugarcane leaf waste ashes on sustainable ultra-high-performance concrete, J. Build. Eng. 72 (2023), 106689, https://doi.org/10.1016/j.jobe.2023.106689, 2023/08/01/.

[4] N.M.S. Hasan, et al., Investigation of lightweight and green concrete characteristics using coconut shell aggregate as a replacement for conventional aggregates, Int. J. Civ. Eng. (2023), https://doi.org/10.1007/s40999-023-00881-x, 2023/08/21.

[5] E. Aprianti, A huge number of artificial waste material can be supplementary cementitious material (SCM) for concrete production–a review part II, J. Clean. Prod. 142 (2017) 4178–4194.

[6] A.M.A. Zeyad, Influence of Steam Curing on Engineering and Fluid Transport Properties of High Strength Green Concrete Containing Palm Oil Fuel Ash, Universiti Sains Malaysia, 2013.

[7] M. Amin, A.M. Zeyad, B.A. Tayeh, I.S. Agwa, Effect of glass powder on high-strength self-compacting concrete durability, Key Eng. Mater. 945 (2023) 117–127, https://doi.org/10.4028/p-w4tcjx.

[8] I.Y. Hakeem, M. Amin, A.M. Zeyad, B.A. Tayeh, I.S. Agwa, K. Abu el-hassan, Properties and durability of self-compacting concrete incorporated with nanosilica, fly ash, and limestone powder, Struct. Concr. (2023), https://doi.org/10.1002/suco.202300121.

[9] A.A.J. Ghanim, M. Amin, A.M. Zeyad, B.A. Tayeh, I.S. Agwa, Effect of Modified Nano-titanium and Fly Ash on Ultra-high-performance Concrete Properties, Structural Concrete, 2023.

[10] M.M.H. Khan, M.H.R. Sobuz, M.M. Meraz, V.W.Y. Tam, N.M.S. Hasan, N.M.N. Shaurdho, Effect of various powder content on the properties of sustainable self-compacting concrete, Case Stud. Constr. Mater. 19 (2023), e02274, https://doi.org/10.1016/j.cscm.2023.e02274, 2023/12/01/.

[11] H. Hamada, B. Tayeh, F. Yahaya, K. Muthusamy, A. Al-Attar, Effects of nano-palm oil fuel ash and nano-eggshell powder on concrete, Construct. Build. Mater. 261 (2020), 119790, https://doi.org/10.1016/j.conbuildmat.2020.119790, 2020/11/20/.

[12] M.S. Fattouh, B.A. Tayeh, I.S. Agwa, E.K. Elsayed, Improvement in the flexural behaviour of road pavement slab concrete containing steel fibre and silica fume, Case Stud. Constr. Mater. 18 (2023), e01720, https://doi.org/10.1016/j.cscm.2022.e01720, 2023/07/01/.

[13] K. Abdelsamie, I.S. Agwa, B.A. Tayeh, R.D.A. Hafez, Improving the brittle behaviour of high-strength concrete using keratin and glass fibres, Adv. Concr. Constr 12 (6) (2021) 469–477.

[14] N.M.S. Hasan, N.M.N. Shaurdho, M.H.R. Sobuz, M.M. Meraz, M.S. Islam, M.J. Miah, Utilization of waste glass cullet as partial substitutions of coarse aggregate to produce eco-friendly concrete: role of metakaolin as cement replacement, Sustainability 15 (14) (2023), 11254 [Online]. Available: https://www.mdpi.com/2071-1050/15/14/11254.

[15] K. Abu el-Hassan, et al., Effects of nano titanium and nano silica on high-strength concrete properties incorporating heavyweight aggregate, Struct. Concr. (2023), https://doi.org/10.1002/suco.202300232.

[16] N.J. Mim, et al., Eco-friendly and cost-effective self-compacting concrete using waste banana leaf ash, J. Build. Eng. 64 (2023), 105581.

[17] M.M. Meraz, et al., On the utilization of rice husk ash in high-performance fiber reinforced concrete (HPFRC) to reduce silica fume content, Construct. Build. Mater. 369 (2023), 130576.

[18] A.M. Maglad, M. Amin, A.M. Zeyad, B.A. Tayeh, I.S. Agwa, Engineering properties of ultra-high strength concrete containing sugarcane bagasse and corn stalk ashes, J. Mater. Res. Technol. 23 (2023) 3196–3218, https://doi.org/10.1016/j.jmrt.2023.01.197, 2023/03/01/.

[19] A. Zeyad, M. Johari, B. Tayeh, A. Saba, Ultrafine palm oil fuel ash: from an agro-industry by-product into a highly efficient mineral admixture for high strength green concrete, J. Eng. Appl. Sci. 12 (7) (2017).

[20] H.M. Hamada, B. Skariah Thomas, B. Tayeh, F.M. Yahaya, K. Muthusamy, J. Yang, Use of oil palm shell as an aggregate in cement concrete: a review, Construct. Build. Mater. 265 (2020), 120357, https://doi.org/10.1016/j.conbuildmat.2020.120357, 2020/12/30/.

[21] E. Khankhaje, et al., On blended cement and geopolymer concretes containing palm oil fuel ash, Mater. Des. 89 (2016) 385–398, https://doi.org/10.1016/j.matdes.2015.09.140, 2016/01/05/.

[22] A. Zeyad, M.M. Johari, N.M. Bunnori, K. Ariffin, N.M. Altwair, Characteristics of treated palm oil fuel ash and its effects on properties of high strength concrete, Adv. Mater. Res. 626 (2013) 152–156.

[23] A.M. Zeyad, M.A. Megat Johari, B.A. Tayeh, M.O. Yusuf, Efficiency of treated and untreated palm oil fuel ash as a supplementary binder on engineering and fluid transport properties of high-strength concrete, Construct. Build. Mater. 125 (2016) 1066–1079, https://doi.org/10.1016/j.conbuildmat.2016.08.065, 2016/10/30/.

[24] H.M. Hamada, G.A. Jokhio, F.M. Yahaya, A.M. Humada, Y. Gul, The present state of the use of palm oil fuel ash (POFA) in concrete, Construct. Build. Mater. 175 (2018) 26–40.

[25] M.A. Megat Johari, A.M. Zeyad, N. Muhamad Bunnori, K.S. Ariffin, Engineering and transport properties of high-strength green concrete containing high volume of ultrafine palm oil fuel ash, Construct. Build. Mater. 30 (2012) 281–288, https://doi.org/10.1016/j.conbuildmat.2011.12.007, 2012/05/01/.

[26] M.Z. Al-mulali, H. Awang, H.A. Khalil, Z.S. Aljoumaily, The incorporation of oil palm ash in concrete as a means of recycling: a review, Cement Concr. Compos. 55 (2015) 129–138.

[27] N.M.S. Hasan, et al., Integration of rice husk ash as supplementary cementitious material in the production of sustainable high-strength concrete, Materials 15 (22) (2022) 8171.

[28] N. Ranjbar, M. Mehrali, U.J. Alengaram, H.S.C. Metselaar, M.Z. Jumaat, Compressive strength and microstructural analysis of fly ash/palm oil fuel ash based geopolymer mortar under elevated temperatures, Construct. Build. Mater. 65 (2014) 114–121.

[29] I.Y. Hakeem, M. Alharthai, M. Amin, A.M. Zeyad, B.A. Tayeh, I.S. Agwa, Properties of sustainable high-strength concrete containing large quantities of industrial wastes, nanosilica and recycled aggregates, J. Mater. Res. Technol. 24 (2023) 7444–7461, https://doi.org/10.1016/j.jmrt.2023.05.050, 2023/05/01/.

[30] N.M. Altwair, M.A.M. Johari, S.F.S. Hashim, A.M. Zeyad, Mechanical properties of engineered cementitious composite with palm oil fuel ash as a supplementary binder, Adv. Mater. Res. 626 (2013) 121–125, https://doi.org/10.4028/www.scientific.net/AMR.626.121.

[31] A.N. Mohammed, M. Azmi Megat Johari, A.M. Zeyad, B.A. Tayeh, M.O. Yusuf, Improving the engineering and fluid transport properties of ultra-high strength concrete utilizing ultrafine palm oil fuel ash, J. Adv. Concr. Technol. 12 (4) (2014) 127–137, https://doi.org/10.3151/jact.12.127.

[32] A.M. Zeyad, M.A. Megat Johari, B.A. Tayeh, M.O. Yusuf, Pozzolanic reactivity of ultrafine palm oil fuel ash waste on strength and durability performances of high strength concrete, J. Clean. Prod. 144 (2017) 511–522, https://doi.org/10.1016/j.jclepro.2016.12.121, 2017/02/15/.

[33] J.-H. Tay, Ash from oil-palm waste as a concrete material, J. Mater. Civ. Eng. 2 (2) (1990) 94–105.

[34] A.M. Zeyad, M.A.M. Johari, A. Abutaleb, B.A. Tayeh, The effect of steam curing regimes on the chloride resistance and pore size of high–strength green concrete, Construct. Build. Mater. 280 (2021), 122409, https://doi.org/10.1016/j.conbuildmat.2021.122409, 2021/04/19/.

[35] A.M. Zeyad, et al., Influence of steam curing regimes on the properties of ultrafine POFA-based high-strength green concrete, J. Build. Eng. 38 (2021), 102204, https://doi.org/10.1016/j.jobe.2021.102204, 2021/06/01/.

[36] H.M. Hamada, A.A. Al-Attar, B. Tayeh, F.B.M. Yahaya, Optimizing the concrete strength of lightweight concrete containing nano palm oil fuel ash and palm oil clinker using response surface method, Case Stud. Constr. Mater. 16 (2022), e01061, https://doi.org/10.1016/j.cscm.2022.e01061, 2022/06/01/.

[37] W. Kroehong, T. Sinsiri, C. Jaturapitakkul, Effect of palm oil fuel ash fineness on packing effect and pozzolanic reaction of blended cement paste, Procedia Eng. 14 (2011) 361–369.

[38] M.M. Johari, A. Zeyad, N.M. Bunnori, K. Ariffin, Engineering and transport properties of high-strength green concrete containing high volume of ultrafine palm oil fuel ash, Construct. Build. Mater. 30 (2012) 281–288.

[39] A. Zeyad, M. Johari, N.M. Bunnori, K. Ariffin, N.M. Altwair, Characteristics of treated palm oil fuel ash and its effects on properties of high strength concrete, in: Advanced Materials Research, vol. 626, Trans Tech Publ, 2013, pp. 152–156.
[40] P. Chindaprasirt, S. Homwuttiwong, C. Jaturapitakkul, Strength and water permeability of concrete containing palm oil fuel ash and rice husk–bark ash, Construct. Build. Mater. 21 (7) (2007) 1492–1499.
[41] V. Sata, C. Jaturapitakkul, K. Kiattikomol, Utilization of palm oil fuel ash in high-strength concrete, J. Mater. Civ. Eng. 16 (6) (2004) 623–628.
[42] W. Tangchirapat, C. Jaturapitakkul, P. Chindaprasirt, Use of palm oil fuel ash as a supplementary cementitious material for producing high-strength concrete, Construct. Build. Mater. 23 (7) (2009) 2641–2646.
[43] B. Alsubari, P. Shafigh, M.Z. Jumaat, Utilization of high-volume treated palm oil fuel ash to produce sustainable self-compacting concrete, J. Clean. Prod. 137 (2016) 982–996, https://doi.org/10.1016/j.jclepro.2016.07.133, 2016/11/20/.
[44] M.M.U. Islam, K.H. Mo, U.J. Alengaram, M.Z. Jumaat, Mechanical and fresh properties of sustainable oil palm shell lightweight concrete incorporating palm oil fuel ash, J. Clean. Prod. 115 (2016) 307–314, https://doi.org/10.1016/j.jclepro.2015.12.051, 2016/03/01/.
[45] B. Alsubari, P. Shafigh, M.Z. Jumaat, Development of self-consolidating high strength concrete incorporating treated palm oil fuel ash, Materials 8 (5) (2015) 2154–2173.
[46] D.-C. Feng, et al., Machine learning-based compressive strength prediction for concrete: an adaptive boosting approach, Construct. Build. Mater. 230 (2020), 117000, https://doi.org/10.1016/j.conbuildmat.2019.117000, 2020/01/10/.
[47] A. Ahmad, et al., Prediction of compressive strength of fly ash based concrete using individual and ensemble algorithm, Materials 14 (4) (2021) 794.
[48] F. Farooq, W. Ahmed, A. Akbar, F. Aslam, R. Alyousef, Predictive modeling for sustainable high-performance concrete from industrial wastes: a comparison and optimization of models using ensemble learners, J. Clean. Prod. 292 (2021), 126032, https://doi.org/10.1016/j.jclepro.2021.126032, 2021/04/10/.
[49] M.A. Khan, S.A. Memon, F. Farooq, M.F. Javed, F. Aslam, R. Alyousef, Compressive strength of fly-ash-based geopolymer concrete by gene expression programming and random forest, Adv. Civ. Eng. 2021 (2021) 1–17.
[50] M.F. Javed, et al., Applications of gene expression programming and regression techniques for estimating compressive strength of bagasse ash based concrete, Crystals 10 (9) (2020) 737.
[51] M.A. Getahun, S.M. Shitote, Z.C.A. Gariy, Artificial neural network based modelling approach for strength prediction of concrete incorporating agricultural and construction wastes, Construct. Build. Mater. 190 (2018) 517–525.
[52] ASTM-C150, Standard Specification for Portland Cement, ASTM International, West Conshohocken, PA., 2020.
[53] A.A. Awal, I. Shehu, M. Ismail, Effect of cooling regime on the residual performance of high-volume palm oil fuel ash concrete exposed to high temperatures, Construct. Build. Mater. 98 (2015) 875–883.
[54] G.F. Huseien, J. Mirza, M. Ismail, M.W. Hussin, Influence of different curing temperatures and alkali activators on properties of GBFS geopolymer mortars containing fly ash and palm-oil fuel ash, Construct. Build. Mater. 125 (2016) 1229–1240.
[55] A.A. Awal, I. Shehu, Performance evaluation of concrete containing high volume palm oil fuel ash exposed to elevated temperature, Construct. Build. Mater. 76 (2015) 214–220.
[56] ASTM-C33, Standard Specification for Concrete Aggregates, ASTM International, West Conshohocken, PA., 2018.
[57] C. Chandara, K.A.M. Azizli, Z.A. Ahmad, S.F.S. Hashim, E. Sakai, Analysis of mineralogical component of palm oil fuel ash with or without unburned carbon, in: Advanced Materials Research, vol. 173, Trans Tech Publ, 2011, pp. 7–11.
[58] W. Sanawung, T. Cheewaket, W. Tangchirapat, C. Jaturapitakkul, Influence of palm oil fuel ash and W/B ratios on compressive strength, water permeability, and chloride resistance of concrete, Adv. Mater. Sci. Eng. 2017 (2017).
[59] T. Xie, P. Visintin, A unified approach for mix design of concrete containing supplementary cementitious materials based on reactivity moduli, J. Clean. Prod. 203 (2018) 68–82.
[60] ASTM-C29M, Standard Test Method for Bulk Density ("Unit Weight") and Voids in Aggregate, ASTM International, West Conshohocken, PA., 2019.
[61] ASTM-C127, Standard Test Method for Relative Density (Specific Gravity) and Absorption of Coarse Aggregate, ASTM International, West Conshohocken, PA., 2015.
[62] ASTM-C128, Standard Test Method for Relative Density (Specific Gravity) and Absorption of Fine Aggregate, ASTM International, West Conshohocken, PA., 2022.
[63] ASTM-C136, Standard Test Method for Sieve Analysis of Fine and Coarse Aggregates, ASTM International, West Conshohocken, PA., 2019.
[64] ASTM-C494, Standard Specification for Chemical Admixtures for Concrete, ASTM International, West Conshohocken, PA, 2020, https://doi.org/10.1520/C0494_C0494M-17.
[65] ASTM-C192, Standard Practice for Making and Curing Concrete Test Specimens in the Laboratory, ASTM International, West Conshohocken, PA, 2015, https://doi.org/10.1520/C0192_C0192M-14.
[66] ASTM-C143, Standard Test Method for Slump of Hydraulic-Cement Concrete, ASTM International, West Conshohocken, PA., 2013.
[67] C. Hu, F. de Larrard, T. Sedran, C. Boulay, F. Bosc, F. Deflorenne, Validation of BTRHEOM, the new rheometer for soft-to-fluid concrete, Mater. Struct. 29 (1996) 620–631.
[68] A.N. Ede, J.O. Agbede, Use of coconut husk fiber for improved compressive and flexural strength of con-crete, Int. J. Sci. Eng. Res. 6 (2) (2015) 968–974.
[69] BS-EN-12350-4, Testing Fresh Concrete-Degree of Compactability, British Standards Institution, London, UK., 2019.
[70] BS-EN-12350-6, Testing Fresh Concrete-Density, British Standards Institution, London, UK., 2019.
[71] ASTM-C39, Standard Test Method for Compressive Strength of Cylindrical Concrete Specimens, ASTM International, West Conshohocken, PA, 2021, https://doi.org/10.1520/C0039_C0039M-21.
[72] ASTM-C496, Standard Test Method for Splitting Tensile Strength of Cylindrical Concrete Specimens, ASTM International, West Conshohocken, PA., 2018.
[73] ASTM-C78, Standard Test Method for Flexural Strength of Concrete (Using Simple Beam with Third-Point Loading), ASTM International, West Conshohocken, PA, 2022, https://doi.org/10.1520/C0078_C0078M-22.
[74] A.M. Zeyad, B.A. Tayeh, A.M. Saba, M. Johari, Workability, setting time and strength of high-strength concrete containing high volume of palm oil fuel ash, Open Civ. Eng. J. 12 (1) (2018).
[75] M. Aldahdooh, N.M. Bunnori, M.M. Johari, Development of green ultra-high performance fiber reinforced concrete containing ultrafine palm oil fuel ash, Construct. Build. Mater. 48 (2013) 379–389.
[76] A.A. Awal, I. Shehu, Evaluation of heat of hydration of concrete containing high volume palm oil fuel ash, Fuel 105 (2013) 728–731.
[77] M.A. Salam, M. Safiuddin, M.Z. Jumaat, Durability indicators for sustainable self-consolidating high-strength concrete incorporating palm oil fuel ash, Sustainability 10 (7) (2018) 2345.
[78] J. Ortiz, A. Aguado, J. Roncero, M. Zermeño, Influencia de la temperatura ambiental sobre las propiedades de trabajabilidad y microestructurales de morteros y pastas de cemento, Concreto y cemento. Investigación y desarrollo 1 (1) (2009) 2–24.
[79] B.S. Thomas, S. Kumar, H.S. Arel, Sustainable concrete containing palm oil fuel ash as a supplementary cementitious material–A review, Renew. Sustain. Energy Rev. 80 (2017) 550–561.
[80] H.M. Hamada, A.A. Alattar, F.M. Yahaya, K. Muthusamy, B.A. Tayeh, Mechanical properties of semi-lightweight concrete containing nano-palm oil clinker powder, Parts A/B/C, Phys. Chem. Earth 121 (2021), 102977, https://doi.org/10.1016/j.pce.2021.102977, 2021/02/01/.
[81] V. Sata, C. Jaturapitakkul, C. Rattanashotinunt, Compressive strength and heat evolution of concretes containing palm oil fuel ash, J. Mater. Civ. Eng. 22 (10) (2010) 1033–1038.
[82] E. Khankhaje, M. Rafieizonooz, M.R. Salim, R. Khan, J. Mirza, H.C. Siong, Sustainable clean pervious concrete pavement production incorporating palm oil fuel ash as cement replacement, J. Clean. Prod. 172 (2018) 1476–1485.
[83] Y. Tambe, P. Nemade, Efficacy of palm oil fuel ash as filler on mechanical properties of aerated concrete, Innovative Infrastructure Solutions 6 (2021) 1–8.
[84] H. Mohammadhosseini, A. Abdul Awal, A.H. Ehsan, Influence of palm oil fuel ash on fresh and mechanical properties of self-compacting concrete, Sadhana 40 (2015) 1989–1999.

[85] R. Siddique, Properties of self-compacting concrete containing class F fly ash, Mater. Des. 32 (3) (2011) 1501–1507.
[86] I. Nikbin, et al., A comprehensive investigation into the effect of water to cement ratio and powder content on mechanical properties of self-compacting concrete, Construct. Build. Mater. 57 (2014) 69–80.
[87] A. J. C. S, Australian Standard, Standards Association of Australia, North Sydney, 2009, 3600-2009.
[88] A. C. Institute, ACI Manual of Concrete Practice, 2017, ACI, American Concrete Institute, 2017.
[89] A. Committee, Building Code Requirements for Structural Concrete (ACI 318-05) and Commentary (ACI 318R-05), American Concrete Institute, 2005.
[90] C. C. J. B. d. I. Euro, International du Beton: CEB-FIP Model Code 1990, Final Draft 1991, 1991 no. 203, pp. 2.1-2.16.
[91] M. Ayub, et al., Promoting sustainable cleaner production paradigms in palm oil fuel ash as an eco-friendly cementitious material: a critical analysis, J. Clean. Prod. 295 (2021), 126296, https://doi.org/10.1016/j.jclepro.2021.126296, 2021/05/01/.
[92] N. Ranjbar, A. Behnia, B. Alsubari, P.M. Birgani, M.Z. Jumaat, Durability and mechanical properties of self-compacting concrete incorporating palm oil fuel ash, J. Clean. Prod. 112 (2016) 723–730.
[93] K. Celik, C. Meral, A. Petek Gursel, P.K. Mehta, A. Horvath, P.J.M. Monteiro, Mechanical properties, durability, and life-cycle assessment of self-consolidating concrete mixtures made with blended portland cements containing fly ash and limestone powder, Cement Concr. Compos. 56 (2015) 59–72, https://doi.org/10.1016/j.cemconcomp.2014.11.003, 2015/02/01/.
[94] M.H.R. Sobuz, S.D. Datta, A.S.M. Akid, Investigating the combined effect of aggregate size and sulphate attack on producing sustainable recycled aggregate concrete, Aust. J. Civ. Eng. (2022) 1–16, https://doi.org/10.1080/14488353.2022.2088646.
[95] M.H.R. Sobuz, et al., Evaluating the Effects of Recycled Concrete Aggregate Size and Concentration on Properties of High-Strength Sustainable Concrete, Journal of King Saud University - Engineering Sciences, 2022, https://doi.org/10.1016/j.jksues.2022.04.004, 2022/04/30/.
[96] G. Hammond, C. Jones, E.F. Lowrie, P. Tse, Embodied Carbon (The Inventory of Carbon and Energy (ICE). Version (2.0)), University of Bath, UK., 2011.
[97] S.C. Bostanci, Use of waste marble dust and recycled glass for sustainable concrete production, J. Clean. Prod. 251 (2020/04/01/2020), 119785, https://doi.org/10.1016/j.jclepro.2019.119785.
[98] T. H, H. A, T. Hemalatha, N. Arunachalam, A. Murthy, N. Iyer, Assessment of embodied energy in the production of ultra high performance concrete (UHPC), International Journal of Students Research in Technology & Management 2 (3) (2014) 113–120.
[99] D. DECC. Guidelines to Defra/DECC's GHG Conversion Factors for Company Reporting, Department of Energy and Climate Change (DECC) and the Department for Environment, Food and Rural Affairs (Defra). [Online]. Available: www.defra.gov.uk/environment/economy/business-efficiency/reporting/.